Journal of Materials Chemistry C

ROYAL SOCIETY OF CHEMISTRY

REVIEW

View Article Online
View Journal | View Issue

Cite this: J. Mater. Chem. C, 2025, 13, 4285

Advances in metal oxide semiconductor gas sensor arrays based on machine learning algorithms

Jiayue Han,[ab] Huizi Li,[ab] Jiangong Cheng,*[ab] Xiang Ma *[c] and Yanyan Fu *[ab]

Received 11th December 2024,
Accepted 27th January 2025

DOI: 10.1039/d4tc05220j

rsc.li/materials-c

Metal oxide semiconductor (MOS) gas sensors have garnered significant attention for their excellent sensitivity and rapid response times. However, distinguishing similar gases in complex environments remains a major challenge. Integrating sensor arrays with machine learning algorithms significantly enhances gas recognition and detection accuracy, making it a key approach for intelligent gas monitoring. This review summarizes recent advances in MOS gas sensor arrays driven by machine learning algorithms. It further explores the mechanisms of MOS/MOS sensor arrays, conventional sensing materials and machine learning algorithms suitable for gas sensor arrays. Additionally, this review reports, summarizes, and evaluates both classical gas sensing algorithms and neural network-based algorithms for gas identification, considering aspects such as operating principles, advantages and disadvantages, and practical applications. In conclusion, this study considers the current landscape and challenges, providing predictions for future research directions. It is hoped that this work will contribute positively to the progression of machine learning-assisted MOS gas sensor arrays and offer valuable insights for gas sensing data processing.

1 Introduction

A sense of smell is vital for perceiving and interpreting our surroundings, aiding in odor detection, scent tracing, and hazard awareness. However, harmful, corrosive, volatile, or flammable gases pose significant health risks beyond the capabilities of natural olfaction. This highlights the critical need for advanced sensing technologies to monitor and identify harmful gases or volatile organic compounds (VOCs), ensuring medical safety, and environmental applications.

Nowadays, gas identification is becoming more and more important in different fields, including ecosystem protection,[1,2] illegal drug detection[3,4] and food quality control.[5–7] As a result, many sensing technologies, such as electrochemical,[8–10] chemical,[11–17] fiber optic[18,19] and capacitive,[20,21] have been applied in these fields. In recent decades, metal oxide semiconductor (MOS) sensors have garnered significant interest for their affordability, high sensitivity, rapid response capabilities, ease of integration, and remarkable stability.[22–28]

The working mechanism of MOS primarily involves several aspects, including their electronic structure, redox reactions, gas adsorption, and ion migration. MOS have a certain band gap, and their conductivity is influenced by oxygen vacancies, doping, and the adsorption–desorption processes of oxygen. Redox reactions can alter their oxidation state, thereby modulating their conductivity. Additionally, oxygen vacancies and defects in MOS can trigger electron migration, changing conductivity and charge carrier concentration. However, such-simple sensing mechanisms often lack gas selectivity, making it hard to identify specific gases. Additionally, since MOS sensors typically operate at elevated temperatures, they suffer from high power consumption and increased sensitivity to environmental factors. This results in low gas selectivity, making it challenging to accurately identify gases using a single sensor.

To solve this drawback of MOS gas sensors, sensor arrays have become a hot topic of recent research.[29] A MOS gas sensor array is composed of a group of independent MOS sensors. Each sensor in sensor arrays is analogous to a receptor that reacts to different odors to varying degrees. The sensor array is able to interact with multiple cross-reacting analytes in the test, eliminating the need to individually extract responses from each sensor. A range of algorithms has been employed to optimize the performance of sensor arrays, leveraging machine learning-based configurations. Recent progress in

[a] State Key Lab of Transducer Technology, Shanghai Institute of Microsystem and Information Technology, Chinese Academy of Sciences, Changning Road 865, Shanghai, 200050, China. E-mail: jgcheng@mail.sim.ac.cn, fuyy@mail.sim.ac.cn
[b] Center of Materials Science and Optoelectronics Engineering, University of the Chinese Academy of Sciences, Yuquan Road 19, Beijing, 100039, China
[c] College of Chemistry and Molecular Engineering, East China University of Science and Technology, Shanghai 200237, China. E-mail: maxiang@ecust.edu.cn

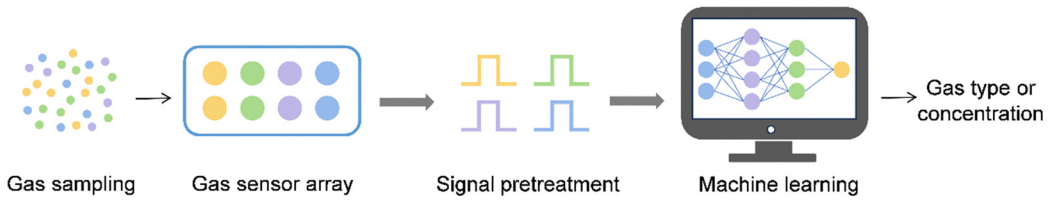

Fig. 1 Schematic illustration of the E-nose system.

computational capabilities and machine learning methodologies has notably improved the precision in gas detection under controlled conditions. The arrays generate variable data sets from complex mixtures, employing different algorithms for further analysis and processing of large amounts of data. These systems decode the convolved signals obtained from gas mixtures into useful information to classify and predict individual gas levels in a mixture, extracting useful and simplified information for the end user. These systems process the mixed signals from a mixture of gases, enabling the classification and prediction of individual gas concentrations, and providing users with clear and concise information for decision-making.

The integration of a gas sensor array with a pattern recognition system is referred to as an electronic nose (E-nose),[30] as shown in Fig. 1. In the E-nose, each sensor responds uniquely to different gases, converting these signals into a collective electrical output. These outputs are then analyzed using pattern recognition techniques, generating distinct signatures for each gas and enabling the identification and prediction of unknown gases. Electronic noses have found applications in several areas, such as environmental monitoring,[31,32] medical diagnosis[33–36] and food safety.[37,38] The qualitative and quantitative gas measurement in artificial olfactory systems is primarily determined by two key factors: the sensor array and the pattern recognition algorithms employed for analysis. Recently, a great deal of research has been invested in gas sensor arrays to improve the accuracy of gas and odor recognition. With the development of the Internet of Things,[39] there is an increasing demand for distributed gas detection, which requires more efficient and intelligent recognition algorithms.

Advancements in large-scale sensor array fabrication and artificial intelligence have enabled machine-learning-assisted optimization to enhance sensor array performance. Machine learning addresses key limitations in gas sensing, such as selectivity, signal drift, and adaptability to complex environments, by extracting patterns from high-dimensional data and improving classification accuracy. Furthermore, adaptive algorithms enable real-time calibration, aging compensation, and precise discrimination of gas mixtures, expanding applications in environmental monitoring, medical diagnostics, and industrial control. This integration marks a transformative step toward next-generation intelligent sensing systems.

Zhiyong Fan's team has developed a high-performance biomimetic olfactory system by integrating large-scale nanotube sensor arrays with advanced artificial intelligence algorithms.[40] The system incorporates up to 10 000 high-sensitivity sensors capable of detecting gases at ppb levels and employs a gradient distribution of MOS materials to achieve a gas classification accuracy of 99.04%. It enables precise identification of gas mixture components and 24 distinct odors. This work addresses the limitations of traditional electronic nose systems, including sensitivity, diversity, and power consumption, and provides a foundation for the development of intelligent sensing and multifunctional systems. Recent progress in computational capabilities and algorithm development has greatly enhanced the precision of gas detection under controlled conditions.[41,42]

The purpose of this paper is to have a comprehensive overview of the gas sensing mechanisms of MOS/MOS sensor arrays, common gas sensing materials and how various emerging machine learning algorithms can assist in the application of MOS gas sensor arrays. Firstly, the gas sensing mechanism of MOS is summarized to reveal the underlying physical changes. Next, we introduce various conventional metal-oxide semiconductor materials. Then, various classical gas sensor algorithms and neural network-based gas sensor algorithms are reviewed. Additionally, we provide a comprehensive comparison of machine learning algorithms for extracting the response of gas sensor arrays. And we introduce various applications of machine learning-assisted data processing of MOS gas sensor arrays. Finally, we offer a perspective on the future advancements and possible applications of MOS gas sensor arrays.

2 Gas sensing mechanism of MOS

The gas sensing mechanism in MOS is predominantly governed by changes in resistivity or conductivity, which occur mainly due to oxygen adsorption. MOS can be categorized into n-type or p-type based on their conductivity characteristics. In n-type semiconductors, such as zinc oxide (ZnO), stannic oxide (SnO_2), indium oxide (In_2O_3) and tungsten oxide (WO_3), negatively charged electrons serve as the primary charge carriers. Conversely, in p-type semiconductors like cupric oxide (CuO), positively charged holes act as the key charge carriers. The gas sensing response typically involves essential processes such as gas chemisorption, charge transfer, and gas desorption. When exposed to air, oxygen molecules adsorb on the sensor surface, where they capture electrons from the conduction band. This leads to the dissociation of oxygen and the formation of oxygen ions through chemisorption, *e.g.* O_{2^-}, O and O^{2-}. The generation of reactive oxygen species reduces the electron concentration and increases the hole concentration. The degree of reactive oxygen species adsorption is largely

influenced by the operating temperature, which is described by the following equation:

$$O_{2(gas)} \rightarrow O_{2(ads)} \quad (1)$$

$$O_{2(ads)} + e^- \rightarrow O_{2^-(ads)} \ (<150\ ^\circ C) \quad (2)$$

$$O_{2^-(ads)} + e^- \rightarrow 2O^-_{(ads)} \ (150\text{–}300\ ^\circ C) \quad (3)$$

$$2O^-_{(ads)} + e^- \rightarrow O^{2-}_{(ads)} \ (>300\ ^\circ C) \quad (4)$$

Under standard atmospheric conditions and typical operating temperatures, oxygen molecules tend to either adsorb or chemically bond to the surface of the sensor. The oxygen molecules capture electrons, creating a space charge layer known as the electron depletion layer. This accumulation of charge results in an expansion of the potential barrier. As a result, due to the reaction of the trapped electrons with the surface gas molecules, the non-intrinsic surface acceptor state of the n-type MOS surface blocks the conduction band electrons. Only a small fraction of electrons can overcome the potential barrier. When a reducing gas interacts with the sensitive MOS surface, it removes the reactive oxygen species from the surface, releasing trapped electrons back into MOS. This process results in a narrowing of the depletion region and a reduction in the bending of the energy bands. Consequently, the resistance of the n-type MOS decreases, while the resistance of the p-type MOS increases. As a result, the presence of reducing gases can be effectively detected by monitoring the changes in the sensor's resistance.

The sensing mechanism of n-type MOS, using ZnO as an example, is depicted in Fig. 2.[43] When ZnO is exposed to air, oxygen molecules adsorb onto its surface and extract electrons from the conduction band, forming reactive oxygen species. Concurrently, an electron depletion layer develops on the surface, leading to a decrease in electron concentration, which narrows the depletion region and raises the sensor's resistance. Upon exposure to NO_2, the NO_2 molecules interact with the adsorbed oxygen species, causing the release of trapped electrons back into the conduction band of ZnO. This increases the electron concentration, causes the depletion layer to expand, and ultimately reduces the sensor's resistance.

Based on the understanding of the gas sensing mechanisms of n-type and p-type MOS, the modification of one material by another can result in various types of junctions, including p–n heterojunctions, n–n homojunctions, p–p homojunctions, and Schottky heterojunctions.[44–46] The formation of the junction causes energy band bending, resulting in a charge depletion region at the interface. This region has a low density of charge carriers, which can be readily depleted by adsorbed oxygen molecules, resulting in a notable change in the gas sensor's resistance. Additionally, dangling bonds and vacancies at the junction create a low charge density state at the interface, further enhancing the sensor's performance. Owing to the formation of dangling bonds and vacancies at the junction, a low charge density state is established at the interface, which enhances the sensing performance. Additionally, synergistic reactions within the heterostructure further improve sensitivity. In this process, one material in the heterostructure may first interact with the target gas or VOCs, while the second material reacts with the byproducts of this reaction. Furthermore, the heterojunction structure, with its high porosity and abundant defect sites, facilitates faster gas adsorption, which contributes to an overall increase in sensor sensitivity.

Among them, p–n heterojunctions have garnered considerable attention due to their ability to control the electron depletion layer thickness. Their formation in sensor materials significantly enhances sensing performance by facilitating charge transfer and improving overall sensitivity.[47,48] For instance, CuO/WO_3 hierarchical hollow microspheres, constructed from irregular two-dimensional nanosheets with a distinct three-dimensional structure, demonstrated superior sensitivity, faster response/recovery times, and better selectivity for xylene.[49] The formation of a heterojunction between CuO and WO_3 is crucial for these enhanced properties. As depicted in Fig. 3, when WO_3 contacts CuO, free electrons move from the

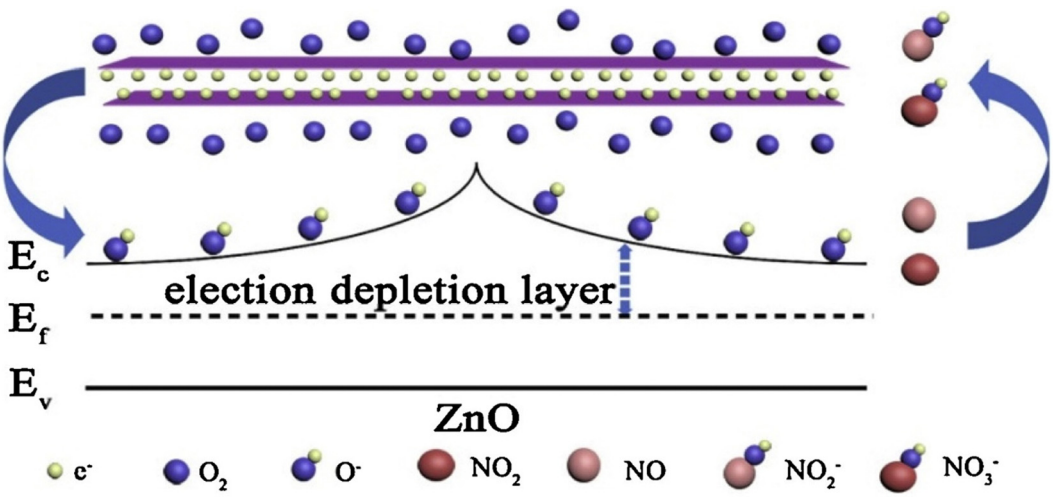

Fig. 2 Schematic illustration of gas sensing mechanism of ZnO. Reproduced from ref. 43 with permission from Elsevier B.V., copyright 2019.

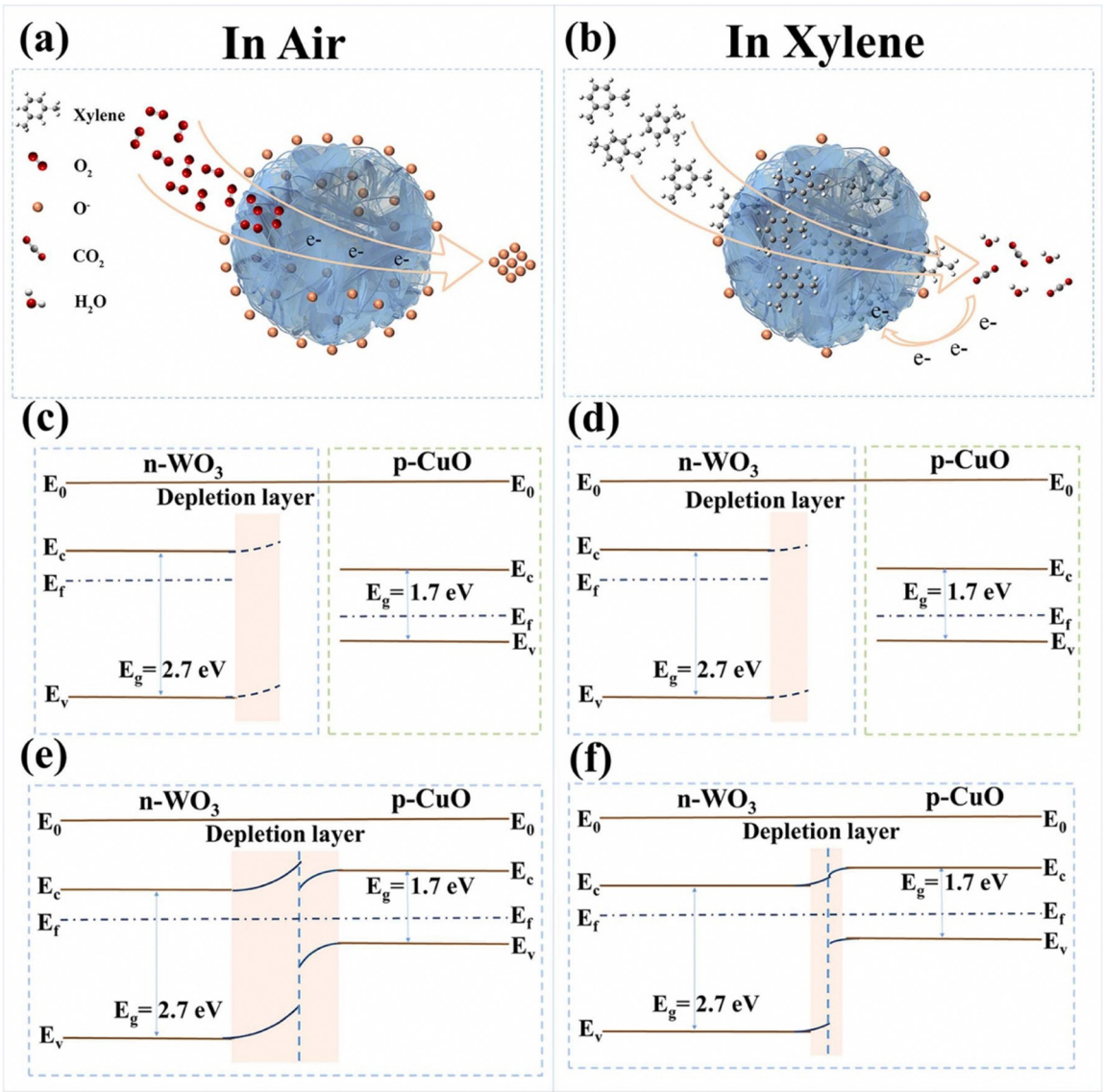

Fig. 3 Schematic illustration of the xylene gas-sensing mechanism on WO_3 and CuO/WO_3 surfaces. (a and b) The gas-sensing mechanism of the CuO/WO_3 surface in air and xylene. (c and d) The energy band structures of WO_3 in air and xylene. (e and f) The energy band structures of CuO/WO_3 in air and xylene. Reproduced from ref. 49 with permission from Elsevier B.V., copyright 2022.

n-type WO_3 to the p-type CuO, while holes migrate in the opposite direction. This charge redistribution continues until the Fermi levels of both materials align, which leads to the expansion of the electron depletion layer. This interaction results in the formation of a heterojunction at the WO_3–CuO interface, thereby increasing the material's resistance.

However, when xylene is introduced, its interaction with reactive oxygen species results in the release of trapped electrons back into the conduction band of WO_3. This process reduces the width of the depletion layer, consequently lowering the electrical resistance of the material. The incorporation of CuO also reduces the agglomeration of the WO_3 nanoparticles, providing adsorption sites for xylene. On the other hand, during the formation of the heterojunction, the mismatch in lattice parameters between the two materials can introduce numerous defects at the interface. These defects act as active sites for gas adsorption, allowing more gas molecules to adhere to the composite surface. Consequently, these adsorbed molecules can interact with reactive oxygen species, promoting reactions with the target molecules.

3 Conventional sensing materials for MOS/MOS sensor arrays

The study of gas sensing using metal oxides began in the 1960s, when Seiyama *et al.* found that the adsorption and desorption of ethanol molecules on ZnO thin films resulted in changes to their electrical conductivity.[50] Since that pioneering work, a wide range of metal oxides have been thoroughly investigated

and are now commonly employed as sensing materials for detecting flammable, toxic, and hazardous gases.

3.1 ZnO

ZnO is a widely used n-type semiconductor with a band gap of 3.37 eV, making it an ideal material for applications such as gas sensors, doped substrates, and composite components. Its appeal lies in its non-toxic, environmentally friendly properties, low cost, and ease of synthesis.

ZnO materials exhibit excellent chemical reactivity and thermal stability, with their morphology playing a crucial role in determining their sensing capabilities. Various ZnO morphologies have been employed for the detection of toxic and hazardous gases.[51–54] Choi *et al.* prepared a porous ZnO nanosheet gas sensing element with good response characteristics to NO_2 gas at 200 °C.[55] The gas-sensing performance of a material is significantly influenced by its specific surface area. As demonstrated in Fig. 4(a), the BET surface area (BET) of porous ZnO nanoparticles is three times higher than that of conventional ZnO nanoparticles. Its highly porous morphology provides abundant pore channels, which leads to a higher response in ZnO nanoparticles gas sensing elements. Moreover, owing to the n-type nature of this gas-sensing material, it contains oxygen vacancies (or metal intermediates).[56] These surface defects provide ideal sites for the adsorption of oxygen and NO_2 gases, thereby enhancing the gas response, as illustrated in Fig. 4(b).

Liu *et al.* designed a highly sensitive triethanolamine (TEA) gas sensor using ZnO ultrathin films that are rich in oxygen vacancies.[57] The response of the gas-sensitive element to TEA is governed by electron transfer through surface redox reactions, as shown in Fig. 4(c) Atmospheric oxygen adsorbs onto the ZnO surface, forming a depletion layer that increases resistance. Upon exposure to TEA, redox reactions release electrons, leading to changes in conductivity. The optimized ZnO thin-film sensor exhibits a high response to TEA concentrations ranging from 21.6 to 10 ppm, with rapid response and recovery times, excellent selectivity, and a low detection limit of 22 ppb.

Moreover, MOS gas sensors are often limited by high detection thresholds, poor selectivity, and slow response and recovery times. Therefore, noble metal functionalized ZnO becomes a sensible choice.[56,58] Liu *et al.* fabricated a high-performance

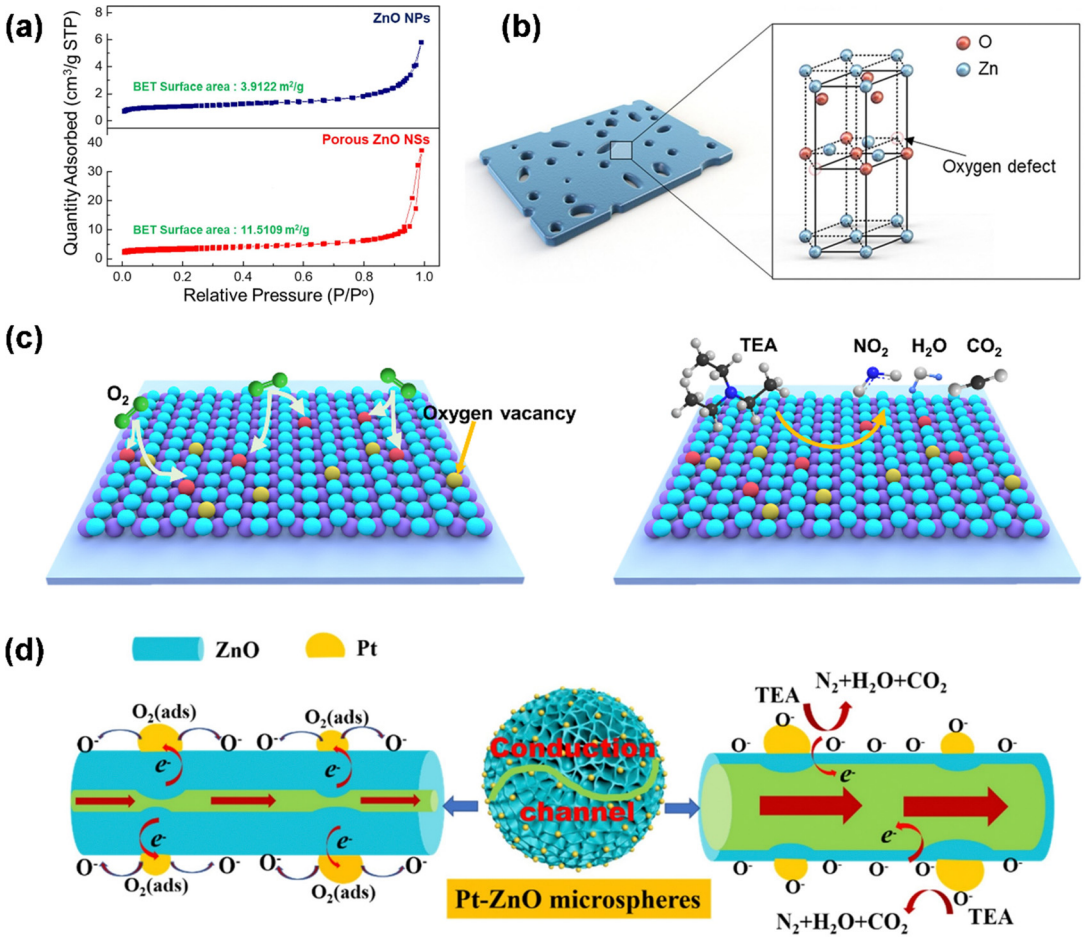

Fig. 4 (a) The BET of ZnO NPs (above) and porous ZnO NSs (below). (b) Effect of surface defects in the porous ZnO NSs gas sensor. Reproduced from ref. 55 with permission from Elsevier B.V., copyright 2021. (c) Surface reaction mechanism of ZnO films in air (left) and TEA (right). Reproduced from ref. 56 with permission from Elsevier B.V., copyright 2021. (d) Schematic diagram illustrating the sensing mechanism of Pt–ZnO microspheres sensor. Reproduced from ref. 57 with permission from Elsevier B.V., copyright 2021.

gas sensor for TEA detection by utilizing Pt–ZnO microspheres.[59] The modification of Pt notably improved the adsorption of active oxygen species on the surface of the composite, which in turn facilitated a greater extraction of electrons from the conduction band of ZnO. This effect, together with the establishment of a Schottky junction, further intensified the electron depletion layer within the Pt–ZnO microspheres, as depicted in Fig. 4(d). The sensor demonstrated excellent selectivity and stability for TEA, with a response range from approximately 242 to 100 ppm. Riek *et al.* developed a gas sensor array using a mixture of metals and organic polymers. The sensitivity of all the gas sensors exceeded 85%, significantly enhancing gas selectivity.[60]

3.2 SnO_2

SnO_2, an n-type semiconductor with a wide band gap ranging from 3.5 to 4.0 eV, has been widely employed in MOS gas sensors since the 1960s due to its remarkable stability and high sensitivity. To enhance the sensing performance of these sensors, significant improvements can be achieved through the development of tailored nanostructures, the creation of nanocomposites, and the application of various surface modification techniques.[61–70]

Li *et al.* synthesized porous SnO_2 nanotubes featuring oxygen vacancies and a large specific surface area. These nanotubes demonstrated superior NO_2 sensing performance at 50 °C, with a quick response time of under 10 seconds, a low detection limit of 0.1 ppm, and remarkable selectivity.[71] Liu *et al.* developed an NH_3 gas sensor by integrating electrospun SnO_2 nanotubes with a composite material consisting of polyaniline and molybdenum disulfide nanosheets, which were further capped with an additional nanosheet layer. At room temperature, the sensor exhibited a response value of 10.9 for 100 ppm NH_3, along with a detection limit of 200 ppb.[72] It also demonstrated fast response and recovery times, excellent reproducibility, good flexibility, and exceptional selectivity. Song *et al.* synthesized heterostructured SnO_2/MO_x nanotubes and nanofibers, and the sensor array constructed using sensors accurately detected ethanol, acetone, and xylene gas mixtures.[73] The gas sensing capabilities of the sensor showed a marked improvement over those of pure SnO_2 nanotubes. These findings underscore the fact that the heterostructure design not only enhances the selectivity of metal oxide-based gas sensors but also facilitates the creation of sensor arrays capable of detecting complex gas mixtures.

Lee *et al.* designed a 3–3 sensor array that integrates three distinct metal oxides—WO_3, SnO_2, and NiO—to create a gas sensor with high sensitivity and selectivity, as illustrated in Fig. 5.[74] This sensor comprises three different nanostructural configurations: thin film and dome-shaped structures, both of which are tested with and without the incorporation of Au nanoparticles. Notably, the dome-shaped nanostructures enhanced the sensor's ability to detect four target gases—acetone, toluene, ammonia, and hydrogen sulfide. Additionally, the inclusion of Au nanoparticles significantly improved the sensor's overall responsiveness. The response of the dome-shaped SnO_2 film with Au nanoparticles to acetone is enhanced by 121 times compared to the original SnO_2 film. This study highlights that the integration of metal oxides with catalysts can lead to the development of gas sensors with enhanced sensitivity and selectivity, making them ideal for targeted applications.

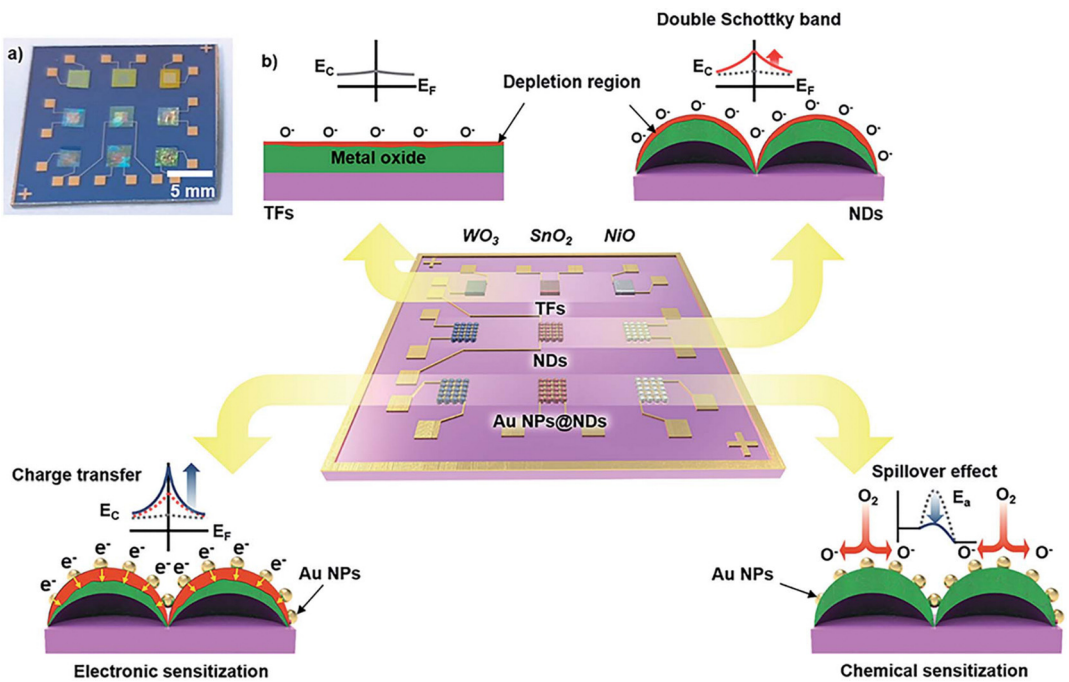

Fig. 5 (a) Digital image of the 3–3 gas sensor array. (b) Schematic representation of the design of the 3–3 gas sensor array. Reproduced from ref. 74 with permission from Royal Society of Chemistry, copyright 2021.

3.3 In_2O_3

In_2O_3 is a significant n-type semiconductor with a direct bandgap ranging from 3.5 to 3.7 eV, offering high electrical conductivity and strong photoelectrochemical stability. Despite these advantages, its use in gas sensing is frequently hindered by issues related to low sensitivity and poor selectivity. To overcome these limitations, several strategies have been explored to enhance the microstructure of In_2O_3, improving its performance in gas detection, aiming to increase its surface area and create more abundant pores, thereby enhancing its gas sensing performance. Up to now, In_2O_3 with various microstructures, such as nanospheres,[75,76] nanosheets,[77] nanorods,[78] and flower-like structures,[79] have been successfully constructed.

Beyond optimizing the structure, various compositional adjustments, including lattice doping, surface treatments, and the creation of heterojunctions, are regarded as effective approaches to enhance the selectivity and sensitivity of MOS. One such approach is the introduction of noble metals onto the surface of In_2O_3 to enhance its response.[80–82] Oh *et al.* prepared arrays of five gas sensors, including pure In_2O_3, three different Cr-doped In_2O_3, and one Cr/Pd co-doped In_2O_3 sensor for five indoor air pollutants were gas-sensitized.[83]

The gas response of In_2O_3 can also be enhanced by engineering specific morphologies or interfaces.[84–86] Li *et al.* successfully combined In_2O_3 with CuO to fabricate a gas-sensitive element that exhibits a strong response to H_2S. The sensor operates effectively at an optimized temperature as low as 70 °C, achieving an 8.5-fold enhancement in response compared to the pure In_2O_3 gas sensor.[87] Zhang *et al.* prepared a 20% ZnO/In_2O_3 hetero structured sensor.[88] Owing to its distinctive hierarchical design, a high density of mesopores, and the creation of n–n heterojunctions, the sensor shows exceptional responsiveness to ethanol gas at 240 °C. For 50 ppm ethanol, the response value reaches 170, which is 3.3 times higher than the performance of the pure In_2O_3-based sensor.

3.4 WO_3

WO_3 is a highly adaptable n-type metal oxide semiconductor with a band gap ranging from 2.6 to 2.8 eV, which makes it an ideal candidate for sensing VOCs and harmful gases. Upon contact with air, oxygen molecules are chemisorbed onto the surface of WO_3, where they capture electrons from the conduction band, resulting in the formation of an electron-depleted layer. The oxygen molecules adsorbed on the surface are subsequently transformed into reactive oxygen species, which actively engage with the molecules of the target gas. This interaction induces a shift in the carrier dynamics; for example, when reducing gases are present, they can react with the reactive oxygen species, leading to the release of the previously captured electrons back into the conduction band.

The gas-sensing performance of pure WO_3 materials can be improved through the control of their structure and morphology.[89–91] The prepared NO_2 gas sensors had a selectivity of high, good stability, good reproducibility and superior response. Park *et al.* designed a sensor array consisting of three individual sensors, each consisting of a layer of WO_3 nanoparticles coated with zeolite, and successfully detected four VOCs—acetone, ethanol, acetaldehyde, and ammonia—at different concentrations.[92] The hierarchical structure of the sensors promotes better gas diffusion and provides more reactive active sites. Therefore, incorporating a three-dimensional hierarchical structure is an effective strategy for enhancing the gas-sensing performance of MEMS-based MOS sensors.

3.5 CuO

CuO, a p-type semiconductor with a narrow band gap of 1.2 to 2.1 eV, has been extensively studied for detecting toxic and flammable gases. However, its high operating temperature, long response time, and low detection limit pose challenges for practical applications. To address these issues, several promising approaches, such as noble metal functionalization, catalysis, and the incorporation of carbon nanomaterials, have been explored to enhance sensor performance. Zheng *et al.* developed a Pd–CuO/rGO sensor with a hierarchical nanowire structure, which showed significantly enhanced response to trace NO_2 gas at room temperature.[93] The abundant active sites created by the porous rGO modification facilitated enhanced gas adsorption and diffusion, while Pd nanoparticles sensitized the CuO substrate, improving the sensor's sensitivity and selectivity.

In addition, the creation of heterojunctions is a promising approach to improving the gas-sensing performance of MOS-based sensors. Yin *et al.* developed graded $CuO@WO_3$ nanocomposites to optimize gas-sensing performance.[94] Under optimal conditions at 100 °C, the 5 wt% $CuO@WO_3$ composite showed a response of 223 to 5 ppm H_2S, 14 times higher than pure WO_3. The formation of a p–p heterojunction further promotes the generation of oxygen molecules, which are then converted into oxygen ions, enhancing the sensing performance of the composite material. Lu *et al.* successfully synthesized Cu_2O–CuO microflowers assembled from nanorods.[95] The Cu_2O–CuO microflower-2 sensor exhibited excellent stability, selectivity, and rapid response and recovery times for NO_2 detection at 187 °C. This sensor shows promising potential for detecting NO_2 at ultra-low concentrations. Huo *et al.* developed graded CuO/NiO nanowall arrays, which exhibited good self-assembly properties.[96] The NiO sensor modified with 2.84 at% CuO showed excellent sensing performance at 133 °C. Compared to pure NiO, the CuO/NiO heterostructure sensor with an optimal composition demonstrated enhanced response to H_2S gas, improved selectivity, significantly reduced recovery time, and a much lower detection limit, enabling real-time monitoring of H_2S at the ppb level.

4 Classical gas sensing algorithms

In the basic architecture of gas sensing algorithms, the main structural modules and commonly used machine learning algorithms from the perspective of signal and data processing

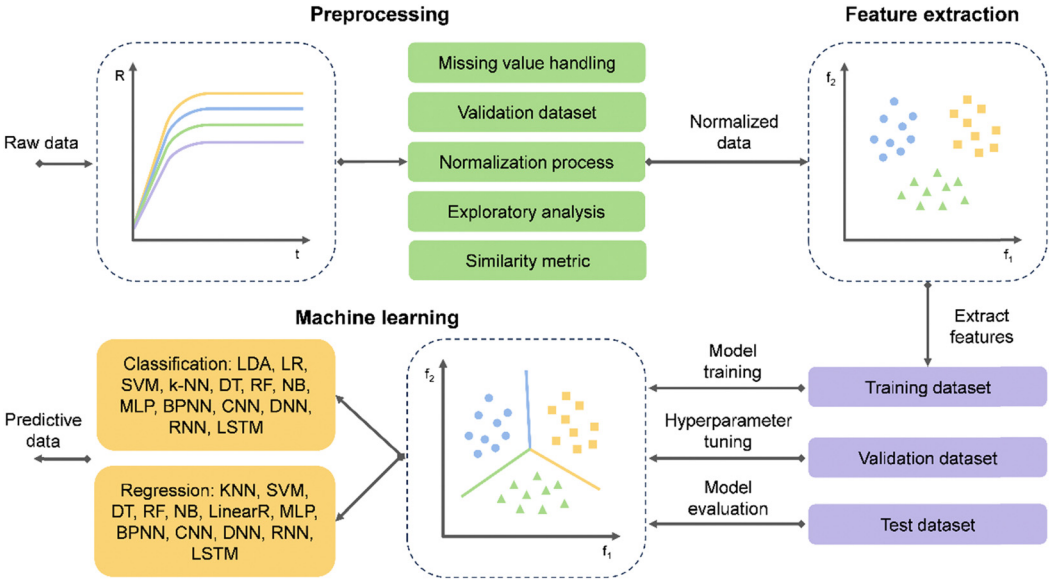

Fig. 6 Schematic illustration of the general process of gas sensing algorithms.

are shown in Fig. 6. First, signal preprocessing of the raw data set is required for bandwidth control and basic feature extraction. The general preprocessing methods include missing value handling, validation dataset, normalization process, exploratory analysis, similarity metrics, and so on. These normalized data will be used for subsequent analysis and feature processing. In machine learning, the data is typically divided into three subsets: training, validation, and test datasets. The training dataset is used to train the model and fine-tune its parameters. The validation dataset is employed to assess the model's performance during training and to optimize hyperparameters. Lastly, the test dataset is used to evaluate the model's ability to generalize and perform on new, unseen data. Based on this, a classifier or regression model is built for gas species identification or concentration prediction.

4.1 Principal component analysis

Principal component analysis (PCA) is a widely used linear, unsupervised technique primarily employed for reducing the dimensionality of a dataset, thereby enhancing its interpretability. It minimizes information loss by retaining the main information in the data. This helps to simplify the data analysis process, reduce computational costs, and filter out noise and redundant information from data. The method works by transforming high-dimensional data into a lower-dimensional space. New feature vectors called principal components (PCs),[97] are used to maximize the explanation of the variance of the original data.

Shooshtari *et al.* created a virtual array for the E-nose by designing four distinct electrodes on the surface of TiO_2.[98] Temperature modulation and discrete wavelet transform were employed to extract new features from the E-nose data. Fig. 7(a) presents a 3D plot that displays the maximum relative amplitudes from each electrode of the electronic nose when exposed to four distinct VOCs. Fourteen distinct features were selected and dimensionality reduction was performed using PCA. The SVM algorithm was used to classify the extracted features, taking advantage of the data's covariance properties. The system successfully classified four different VOC gases, achieving an impressive classification accuracy of 97.5%, as shown in Fig. 7(b). However, some overlap occurred between gases, with a 2.5% misclassification rate, as shown in Fig. 7(c). Despite this, the error rate is minimal and does not impact overall accuracy. Filianoti *et al.* analyzed VOCs for the diagnosis of urological diseases using an electronic nose.[99] Prostate cancer patients were successfully differentiated from healthy controls through PCA, as shown in Fig. 7(d).

The core idea of PCA is to reduce the dimensionality of high-dimensional data through linear transformations, mapping it into a lower-dimensional space, thus enabling data reduction and feature extraction. When reducing the size of the dataset, it is often necessary to sacrifice the accuracy of the data to a certain extent. The principle is to trade some precision for more concise data structures. A streamlined dataset is easier to analyze further and also allows for easier and faster processing of the data without the need to introduce additional variables. However, despite its excellent dimensionality reduction capabilities, PCA has some limitations and is unable to separate subsets when dealing with smaller datasets. PCA is particularly important when sensor arrays detect multiple analytes. It centers on the use of feature vectors to guide the construction of a new feature space, where the magnitude of these vectors reflects the sensor array's response to a specific analyte. Using PCA techniques, gas sensor arrays are able to simultaneously extract and record data for multiple cross-reactive gases, which is difficult to achieve with individual sensors.

4.2 Linear discriminant analysis

Linear discriminant analysis (LDA) is a widely used supervised learning method, primarily applied for dimensionality

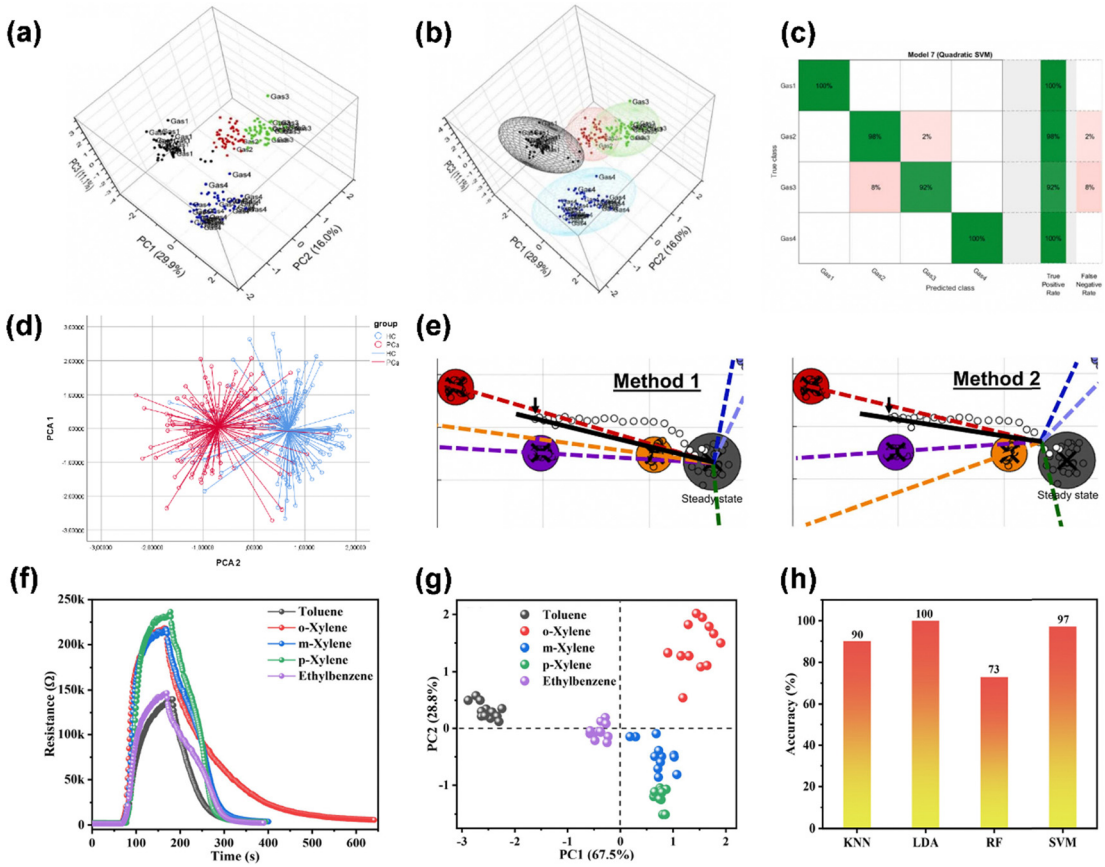

Fig. 7 (a) Results from the exposure of the 4-electrode array to four different VOC vapors. (b) Classification of the PCA 3D plot using the SVM algorithm. (c) Accuracy of the SVM classification shown in the truth table. Reproduced from ref. 98 with permission from Elsevier B.V., copyright 2022. (d) 2D PCA analysis plot showing that prostate cancer patients can be distinguished from healthy controls. Reproduced from ref. 99 with permission from MDPI, copyright 2022. (e) The discrimination model for the target gas in the direction of the LD score from the reference point to the test data. Reproduced from ref. 101 with permission from Elsevier B.V., copyright 2023. (f) Response and recovery curves of a single 3-Ti-Co_3O_4 sensor for 50 ppm of five gases at 280 °C. (g) PCA analysis of features from the response–recovery curve dataset. (h) Comparison of classification accuracy using KNN, LDA, RF, and SVM classifiers. Reproduced from ref. 102 with permission from American Chemical Society, copyright 2022.

reduction and the classification of reduced data. Its core principle is to effectively separate data by projecting the dataset into a low-dimensional space with distinct categorical features. The variance of different categories in the projected feature space is maximized, while the intra-category variance is minimized. It helps to extract key features and reduce the complexity of the data.

Similar to PCA, LDA is a multivariate data analysis method that aims to construct feature sets that effectively capture the underlying characteristics of the input data. However, LDA chooses the projection direction that best improves classification performance, whereas PCA focuses on the direction with the highest variance after sample projection. LDA utilizes the category information to expand the distance between different categories, thus improving the signal-to-noise ratio and classification performance. Sberveglieri *et al.* utilized LDA to analyze VOCs in three types of fruit flavors and five recipe profiles, investigating the aromatic fingerprint characteristics of jams.[100]

However, LDA has some limitations, which mainly depend on the size and dimensionality of the training dataset. For effective classification and dimensionality reduction, LDA usually requires a sufficiently large sample size, otherwise it may lead to overfitting or underfitting problems. When the dimensionality of the dataset is high, the dimensionality catastrophe problem may be encountered. It leads to challenges such as increased computational complexity and reduced model generalization capability. Itoh *et al.* developed an LDA-based identification method for analyzing sensor arrays, capable of distinguishing various target gases under polluted and clean air conditions in the LDA space.[101] Fig. 7(e) illustrates the improved LDA directional discrimination model. In Method 1, the reference point is established based on the steady-state significance observed in the training data. In Method 2, the reference point is defined by the linear discriminant score of the test data, which is the first to deviate from the steady-state region.

Furthermore, LDA creates the classifier by choosing dimensions that maximize the ratio of variance between classes to variance within classes, thereby improving its ability to distinguish between classes, particularly in low-dimensional spaces. Dong *et al.* used Ti-doped Co_3O_4 sensors for gas recognition of aromatic compounds.[102] Due to the varying surface redox rates of the Ti-doped Co_3O_4 sensor, the aromatic gases exhibited

distinct response characteristics, as shown in Fig. 7(f), providing an opportunity for algorithm-based identification. Excellent grouping was achieved through PCA, as illustrated in Fig. 7(g), showing clear separation of toluene, xylene isomers, and methane. The feature vectors obtained from PCA were used as inputs for KNN, LDA, RF, and SVM classification algorithms. Fig. 7(h) presents the prediction accuracy of the four classification algorithms. Notably, LDA achieved a classification accuracy of 100% for aromatic compounds, successfully enabling their chemical identification.

4.3 Support vector machine

Support vector machine (SVM) is a supervised learning algorithm that utilizes a mathematical model to maximize the margin between two classes in a given dataset. When new data points are added to the training set, they are classified based on their position relative to this hyperplane. The key idea behind SVM is to prioritize data points according to their distance from the decision boundary. Points near the decision boundary, called support vectors, are crucial for defining the classification boundary, while points farther away have less influence.

In the gas sensor array, SVM functions as an optimization tool to determine the most effective decision boundary, allowing for the classification of the two datasets into separate groups. The algorithm achieves classification of different gas types or concentrations by using features in the training dataset to classify samples of different gases into two or more classes to build a gas classification model. SVM uses only a single data point and predicts the next data point through multiple iterations. Smaller datasets do not affect the accuracy of the predicted data and are not limited by covariance information. Meng *et al.* improved the selectivity of gas sensors by combining Z-shaped rectangular wave temperature modulation with the SVM algorithm, demonstrating superior capability of SVM in handling small sample sizes.[103] SVM has better generalization ability, which LDA and PCA cannot do. Gerhardt *et al.* employed LDA and SVM to distinguish between different categories of extra virgin olive oil.[104] While the SVM method outperformed the linear LDA method, the overall accuracy improvement was only 5%. It is because SVM is not suitable for large datasets. SVM is effective in dealing with either linear or nonlinear discriminative problems, but when the dataset contains both complex linear and nonlinear relationships, the method cannot perform effectively. In addition, SVM does not perform well with datasets that are incomplete or contain noise. Researchers often use two or more algorithms to improve accuracy. Meng *et al.* used raw data as input for the SVM, achieving 100% accuracy in gas type identification. After successfully identifying gas types, PCA was applied for data dimensionality reduction, with a relative error of approximately 5%.[105]

4.4 k-Nearest neighbors

k-Nearest neighbors (k-NN) is a widely used supervised learning algorithm for classification and regression tasks. In classification, k-NN identifies the k nearest neighbors by calculating Euclidean distances between the input data point and all points in the training dataset. It then assigns the class label based on a majority vote from the neighbors. The simplicity of the algorithm and its ease of implementation make k-NN a suitable choice for a variety of algorithm problems. Moreover, since the decision boundary of k-NN is nonlinear, it is better than linear classifiers in dealing with data classification problems with irregular boundaries.[106] Yun *et al.* used k-NN to analyze 22 tea compounds that were present in the samples in order to determine the origins of black tea, and the k-NN identified 100% of the aroma constituents from nine origins.[107] However, the k-NN algorithm has low data tolerance and high dependence on the quality and balance of data samples, which can affect the prediction accuracy if there are erroneous samples in the training data is not balanced.

4.5 Decision tree and random forest

Decision tree (DT) is a tree-based model widely applied to classification and regression tasks. It provides good decision support by quickly and efficiently decomposing a complex decision process into a series of simple decisions. It automatically selects features and reduces complexity, and constructs decision trees by recursively dividing the dataset into purer, more homogeneous subsets. Each tree is made up of nodes and leaves, where each node represents a parameter and compares its value to a threshold. This comparison determines the direction the tree takes, ultimately leading to a leaf node that corresponds to a specific category. The final classification result is obtained by summing the activated leaves from all the trees. In principle, by utilizing the properties of gases (*e.g.*, toxicity, flammability, density, *etc.*), it is possible to decompose the complex task of multi-gas identification into several simple tasks.

Random forest (RF) is an ensemble method that combines predictions from multiple decision trees to reduce overfitting. While a single tree cannot provide effective results, Random forest improves the learning ability of the model by increasing the number of trees. However, the training time increases proportionally with the number of trees in the random forest. These decision trees work by designing tree-like classifiers, where each node is determined by features chosen based on maximizing information gain. The estimated parameter represents the total number of trees in the forest, while the maximum depth refers to the number of levels or layers within each tree, and the final result is the average of all tree decisions. Random forests improve the stability and accuracy of the model by randomly selecting the sensor responses, calculating the weights of each sensor and averaging them. Kanaparthi *et al.* predicted NH_3, CO_2 and H_2S with 99.8% accuracy using RF classification algorithm.[108] Wang *et al.* used the random forest algorithm to achieve 99% accuracy in identifying VOC vapor species.[109]

5 Neural network based gas sensing algorithm

Neural networks (NN) are powerful machine learning based classifiers that specialize in nonlinear mapping. Neural

networks replicate the information processing behavior of animal brains, utilizing distributed and parallel processing. By adjusting the connections between numerous internal nodes, they harness the system complexity to effectively process information. Neural networks have proven to be ideal for complex gas recognition tasks. Compared with classical gas sensing algorithms, it can improve the recognition accuracy by adjusting the number of layers, the number of neurons in each layer, the choice of activation function, and the associated parameters. In general, the richer the gas data samples are, the better the recognition results of the neural network will be.

5.1 Multilayer perceptron

Multilayer perceptron (MLP) is a feed-forward neural network consisting of multiple layers of neurons, which is a basic artificial neural network model (ANN). It has excellent nonlinear mapping and generalization capabilities. MLP consists of three or more layers, including an input layer, an output layer, and one or more hidden layers, as shown in Fig. 8. MLP employs a nonlinear activation function for its neurons, with each layer being fully connected to the subsequent layer. By integrating multiple perceptrons and employing nonlinear or linear activation functions to define decision boundaries, each perceptron offers a nonlinear mapping in a higher-dimensional space. A neuron is activated when the weighted sum of its inputs exceeds the threshold defined by the activation function. The output is passed through successive layers of neurons until it reaches the output layer. During the training phase, both the activation function parameters and the connection weights are optimized. The backpropagation algorithm minimizes the global error between the network's predicted output and the actual target values. Tang *et al.* utilized an MLP-based hybrid deep neural network for environmental compensation to address sensor drift caused by external factors. Their innovative architecture, combining CNN and MLP, boosted classification accuracy to 95%.[110]

Due to its nonlinear mapping capability, high parallelism, and global optimization features, MLP has demonstrated significant success in areas such as image processing, predictive systems, and pattern recognition. Geng *et al.* used MLP and PCA to differentiate ammonia from other gases at four different concentrations, respectively.[111] The results demonstrated that PCA is inferior to MLP in terms of gas recognition accuracy. However, MLP can be inefficient in high-dimensional spaces, which may result in overfitting. Moreover, the presence of hidden layers increases the number of hyperparameters, making the training process more computationally intensive and leading to slower convergence. In the traditional MLP model, each neuron can only receive a single real number of data inputs, and thus is ineffective in dealing with multidimensional signal inputs. Zhai *et al.* developed a high-precision MLP based on an array of SnO_2 gas sensors for solving the nonlinear problem in odor recognition with an accuracy of 97.4%.[112]

5.2 Backpropagation neural network

Backpropagation neural network (BPNN) is a multilayer feed-forward neural network with a forward structure, widely used in pattern recognition and quantitative prediction. BPNN consists of input, hidden, and output layers, with complete internal connectivity between the upper and lower layers and the ability to adjust the connection weights of each layer through data-driven learning. The input vector is multiplied by initial weights and passed through the activation function to the next layer, reaching the output neuron. The loss function computes the difference between the output and true value. Using the

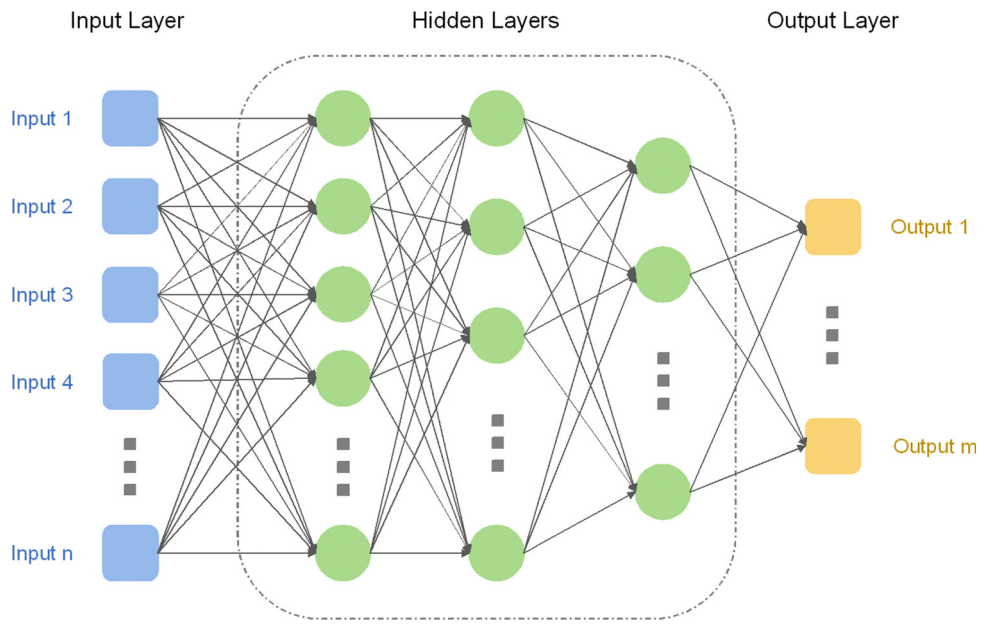

Fig. 8 Schematic illustration of MLP network.

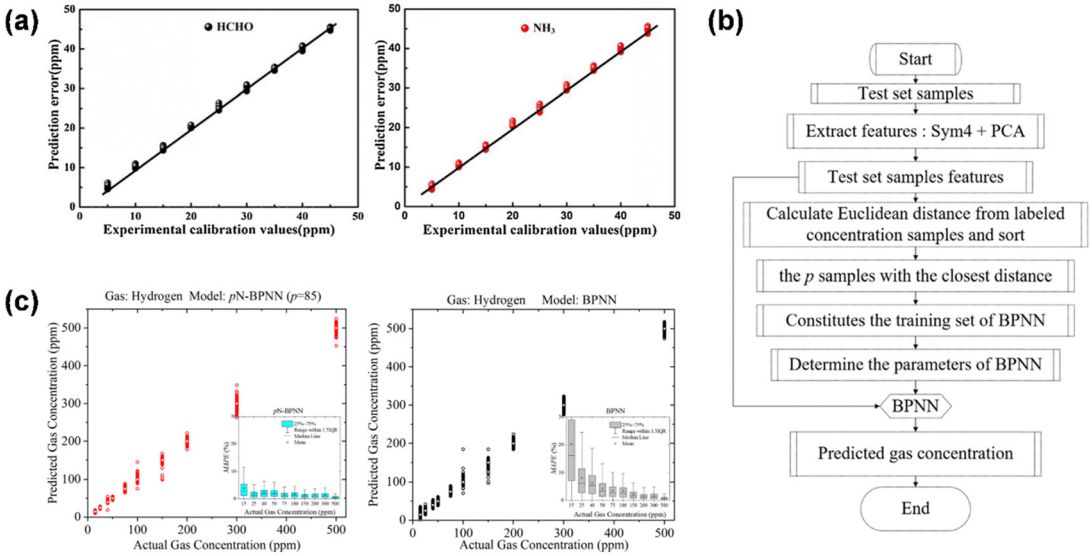

Fig. 9 (a) Curve fitting of the prediction and actual values. HCHO (left); NH_3 (right). Reproduced from ref. 113 with permission from Elsevier B.V., copyright 2021. (b) The flowchart of the ρN-BPNN model for concentration estimation. (c) The predictions of ρN-BPNN (left), and BPNN (right) for each concentration of hydrogen. Reproduced from ref. 116 with permission from Elsevier B.V., copyright 2023.

chain rule, the weights are updated iteratively to optimize the model towards a local optimal solution.

The application of BPNN in gas identification has gradually grown recently. Song *et al.* quantitatively detected and predicted the composition of formaldehyde and ammonia mixtures using sensor arrays and BPNN algorithms.[113] Fig. 9(a) shows the BP–NN results used to predict formaldehyde and NH_3 concentrations in the mixture. The vertical coordinates indicate the predicted values and the horizontal coordinates indicate the experimentally calibrated values. As shown, mixture components predicted by neural networks agrees with the experimental calibration values with a prediction error of <0.8 ppm.

However, there are some limitations in BPNN. BP neural networks are typically nonlinear algorithms, and may have local minima, which makes it difficult for global optimal solution search.[115] In the case of large sample data, the mean-square error is too large and it is difficult to converge. Wang *et al.* designed an improved deep BP neural network to reduce the influence of environmental factors on the accuracy of NO_2 detection, and achieved accurate monitoring in the complicated environment.[114]

Li *et al.* developed a ρ-nearest BPNN (ρN-BPNN) model, as illustrated in the flowchart in Fig. 9(b).[116] The model works by training the BP neural network to estimate gas concentration using the ρ nearest samples from the training set to the test sample. This method reduces the influence of distant samples, thereby improving the model's accuracy. The ρN-BPNN model effectively estimates gas concentrations, achieving an average absolute percentage error of 15–500 ppm for hydrogen detection. Fig. 9(c) shows the prediction of ρN-BPNN and BPNN for each hydrogen concentration in 100 experiments. The inset shows the distribution of absolute errors for each hydrogen concentration. The ρN-BPNN model exhibits more stable estimation performance and higher accuracy for low-concentration samples compared to the standard BP neural network. With standard deviations of 9.31% for BPNN and 4.72% for ρN-BPNN, the latter demonstrates better stability and precision.

5.3 Convolutional neural network

Convolutional neural network (CNN) is a fundamental and widely utilized model in the deep learning. The local connectivity, weight sharing and down-sampling properties of CNN enable it to exhibit sample invariance and show great robustness in dealing with translations, scaling and distortions.[117] The key difference between CNN and traditional BPNN lies in weight sharing and local connectivity. Weight sharing makes CNN architecture more akin to biological neural networks, while local connectivity reduces model complexity and the number of parameters. The basic CNN structure is shown in Fig. 10. The convolutional layer generates a feature map from the input data by applying multiple convolutional filters. Through the features of local connectivity, parameter sharing and multiple convolutional kernels, more features can be extracted using fewer parameters when extracting data features compared to a fully connected layer. In addition, CNN extracts feature in the convolutional and pooling layers, and then the fully connected layer obtains high-level classification information by integrating the feature maps output from the convolutional layer, and performs data classification and output.

CNNs extracts local gas features through convolution, but they do not capture the global correlations between these features.[118,119] Kang *et al.* employed glancing angle deposition (GLAD) technology to create a gas sensor array with consistent sensing performance on a silicon wafer, as shown in Fig. 11(a).[120] The array utilized SnO_2, In_2O_3, WO_3, and CuO

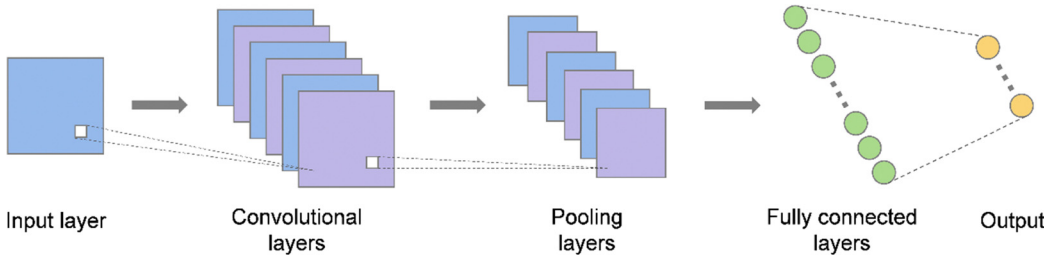

Fig. 10 Schematic illustration of the CNN structure.

for the MOS gas sensors, as illustrated in Fig. 11(b). To meet the high-temperature requirements of low-power MOS sensors, a MEMS-based suspended microheater platform was integrated. The sensor data was processed using CNN in matrix form for selective gas detection, incorporating both the sensor array and the temporal patterns of gas responses. By applying the CNN to the preprocessed data within a moving time window, transient data was effectively leveraged for real-time gas detection, even for gases not included in the training algorithm, as shown in Fig. 11(c).

At present, the application of CNN in gas recognition is gradually developing.[121] Li *et al.* developed a CNN-based high-sensitivity breath ammonia detection system, achieving high precision and sensitivity in decay time extraction.[122] With the development of computer vision, CNN has shown excellent performance in image recognition. Therefore, as long as we convert the sensor response curve into an image, we can distinguish various gases with the help of CNN. Han *et al.* converted time-series data into an image-like matrix for CNN parameter tuning, achieving a gas recognition rate of 96.67%. This approach provides a novel method for classifying mixed gas data.[123] However, CNNs demand large, diverse training datasets. A small or imbalanced dataset can lead to overfitting, reducing the model's generalization ability. Wei *et al.* developed a LeNet-5 convolutional neural network structure for recognizing CO, CH_4 and their mixed gases, and the gas recognition accuracy reaches 98.67%, which further improves the gas classification accuracy and avoids the overfitting problem.[124]

6 Machine learning assisted gas sensing data processing

With the diversification of gas sensing materials and gas sensing mechanisms, the substantial improvement of sensing

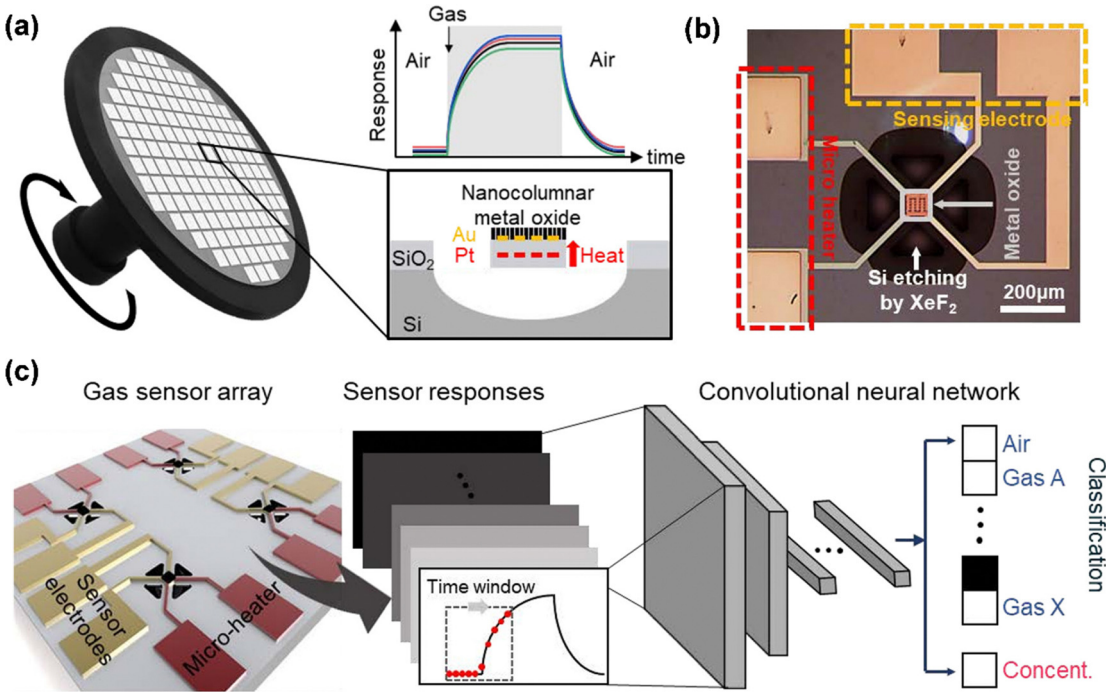

Fig. 11 (a) Schematic illustration of the fabrication process for high batch-uniform MOS gas sensors using GLAD. (b) Microscopic image of MOS gas sensors with a suspended microheater platform. (c) Real-time classification and regression of target gases using CNN-based analysis of gas sensor data. Reproduced from ref. 120 with permission from American Chemical Society, copyright 2022.

performance, and the miniaturization of devices, MOS gas sensor devices are rapidly developing towards large data volumes and high-level features. This trend opens up broad prospects for realizing smarter and more sensitive gas sensors. However, traditional data processing techniques are overwhelmed in coping with the massive amount of sensing data, which usually requires manual intervention, complex and time-consuming processes. To overcome these challenges, a machine learning approach to assist gas sensor array technology data processing can effectively accelerate the process. Machine learning not only has the ability to process high-dimensional and non-linear data, but also can mine complex or hidden relationships from massive data sets, thus significantly improving the efficiency and accuracy of data analysis. This approach automates the extraction of important features, such as sensor response patterns, sensitivity, selectivity, and signal-to-noise ratios, and optimizes the performance of sensor arrays, making them more resilient in complex environments.

Moreover, the inherent low selectivity of MOS sensors has been a major bottleneck in their applications, especially when confronted with multiple gas compositions that are prone to interference. With machine learning algorithms, the sensors are not only able to overcome the lack of selectivity, but also enhance the ability to recognize specific gases. ML algorithms can also neutralize multiple interferences, such as fluctuations in environmental conditions and cross-talk between different gases. Yang *et al.* used two convolutional neural networks to compensate for the effect of ambient temperature variations on H_2 concentration prediction.[125] Comparison with single hidden layer BPNN and double hidden layer BPNN showed that the CNN model had the smallest error in predicting the concentration. 12.3% for concentrations below 1 ppm and 5.7% for concentrations above 1 ppm.

In the design of a smart electronic nose system, choosing a suitable gas sensing algorithm is one of the key steps. The selection of an algorithm is typically based on the characteristics, dimensions, and volume of the sensor data. Different gas sensing tasks involve a variety of complex chemical compositions and multidimensional data, which makes the demand for algorithms diverse. To meet this challenge, the selection of gas recognition algorithms should not only consider the characteristics of the data, but also the processing power and real-time performance.

Among the gas sensing algorithms discussed above, classical gas sensing algorithms and neural network-based gas sensing algorithms have their own advantages. In Table 1, the main attributes of these algorithms are summarized and compared to better understand the applicable scenarios and performance differences of each algorithm. For example, certain classical algorithms are good at handling high-dimensional gas data containing multiple chemical features, and achieve efficient identification by extracting important features in the data. Neural network-based algorithms, on the other hand, are better suited to deal with sensor data with large fluctuations due to their strong adaptive learning capability, thus maintaining high recognition accuracy in dynamic environments. In addition, neural network algorithms perform particularly well in dealing with complex nonlinear data, and are able to capture potential relationships that are difficult to be discovered by traditional algorithms. Zheng *et al.* developed a genetic algorithm-tuned neural network model to analyze the gas sensing responses of SnO_2, ZnO, In_2O_3, NiO, and Cr_2O_3 to eight VOCs, achieving optimal performance.[126] Ren *et al.* developed a 4-sensor array for the trimethylamine detection.[127] BPNN and PCA-based linear regression models were trained using gas-sensing data to achieve accurate identification of different gases. The predictions of BPNN were very close to the actual gas concentrations, while the predictions of PCA-LR model deviated from the true values. Each algorithm has its advantages and disadvantages which should be carefully evaluated in different situations. Choosing the right algorithm is essential, as it can greatly improve the system's overall performance.

Therefore, machine learning-assisted MOS gas sensor arrays are increasingly employed in environmental monitoring, medical diagnostics, and food safety analysis, as shown in Table 2. These systems aid in monitoring air quality, detecting harmful gases, assisting in disease diagnosis through VOC detection, and ensuring food safety by identifying pollutants. These diverse applications highlight the essential role of algorithms in improving the capabilities of MOS gas sensors and demonstrate its potential to advance gas sensing technologies. However, despite the significant progress made in integrating gas sensing technologies with machine learning algorithms, the development of smart electronic nose systems still faces several unavoidable challenges.

While machine learning enables systems to automatically integrate information and learn from experience to improve prediction accuracy, it is difficult to avoid the limitations inherent in machine learning-based data processing with its algorithms. First, for the purpose of assure the predictive

Table 1 Comparisons of machine learning algorithms

	Property	Efficiency	Data demand	Precision	Robustness	Interpretability
PCA	Unsupervised	Fast	Low	Low	Moderate	High
LDA	Supervised	Fast	Low	Low	Moderate	Moderate
SVM	Supervised	Moderate	Moderate	Moderate	Low	Moderate
k-NN	Supervised	Slow	High	Moderate	Moderate	Low
DT/RF	Supervised	Moderate	Moderate	Low	Low	High
MLP	Supervised	Moderate	High	High	Low	Low
BPNN	Supervised	Slow	High	High	Moderate	Low
CNN	Supervised	Slow	High	High	High	Moderate

Table 2 Applications of machine learning algorithms in gas sensor arrays

Field	Applications	Sensors number in the array	ML algorithms	Precision (%)	Target gases	Ref.
Environmental monitoring	Air quality assessment	4	CNN	94.55	NO_2, CO	128
	Combustible/hazardous gas identification	5	k-NN, SVM, RF	97.54	C_4H_{10}, CH_4, C_3H_8, H_2	129
	Indoor VOCs testing	16	k-NN, ANN, DT, RF, SVM	98.75	NH_3, CH_3CHO, C_3H_6O, C_7H_8, ethanol, C_2H_4	130
	Vehicle exhaust pollution detection	4	SVM	96	NO, NO_2, NH_3, C_3H_8	131
	Pest control	4	PCA, LDA, SVM, k-NN, PNN	97.62	Plants volatile organic compounds	132
	VOCs gas analysis	6	SVM, ANN	97.9	CH_2O, ethanol, toluene, C_8H_{10}	133
Medical diagnostics	Diabetes testing	7	PCA, MVRVM	99.72	Acetone, ethanol	134
	Asthma testing	32	PCA	70.4	VOCs	135
	Non-invasive prediction of lung cancer	6	PCA, DFA	98.6	VOCs	136
	Lung cancer detection	19	SVM	94.25	VOCs	137
	Gas detection	16	CNN	98.75	NH_3, CH_3CHO C_3H_6O, C_2H_4, ethanol, toluene	138
	Non-invasive detection of lung cancer	5	SVM, k-NN	92.3	VOCs	139
Food safety analysis	Wine quality rapid detection	6	MLP	96.34	Acetic acid	140
	Beer quality assessment	9	ANN	97	Ethanol, CH_4, CO, NH_3, H_2S, H_2	141
	Infested rice detection	32	PCA	90	VOCs	142
	Identification of essential oils from herbs and fruits	9	PCA, SVM, LDA	98	VOCs	143
	Moldy apples recognition	10	BPNN	96.3	CH_4, H_2S, NO_2	144
	Chicken meat classification	6	RF	98.42	NH_3, TMA, H_2S	145

Note: probabilistic neural network (PNN); multivariate relevance vector machine (MVRVM); discriminant function analysis (DFA)

model accuracy, the sensing system requires a large, diverse, and rigorously filtered amount of training data, a process that is both cumbersome and time-consuming. In addition, due to inherent shortcomings, the behavior of gas sensors never stabilizes over time, which makes the repeatability problem particularly acute. This problem is directly related to model training, thus significantly increasing the difficulty of integrating machine learning algorithms. Therefore, it is particularly important to develop smarter machine learning algorithms to simplify the training steps and improve the sensor performance (especially stability and sensitivity). Wang *et al.* proposed combining a surface state model with a GRU-based regression method to enhance the analytical capabilities of gas sensor data.[146] Liu *et al.* developed a soil nutrient content prediction model combining electronic sensing and machine learning.[147] An E-nose system with 10 gas sensors was used to monitor soil pyrolysis gas concentrations. To predict soil nutrient content, SVM, RF, MLP, and MLP-RF models were applied, with the MLP-RF model outperforming the others.

7 Conclusion and outlook

This paper provides an overview of recent advances in MOS gas sensor arrays based on machine learning algorithms. Based on sensor arrays, the basic gas sensing mechanism of MOS is discussed and various common MOS sensing materials are described. Machine learning algorithms applied to MOS gas sensor arrays are reviewed, covering gas algorithms and neural network-based gas sensing methods. A comprehensive comparison of various machine learning algorithms used to extract the response of gas sensor arrays is presented, and a variety of studies of machine learning-assisted data analysis of MOS gas sensor arrays are described.

With the rapid advancements of semiconductor and machine learning technologies, MOS gas sensor arrays based on machine learning algorithms are poised for further advancements in the following aspects.

(1) MOS gas sensors are still facing challenges such as high power consumption, environmental susceptibility and limited selectivity. Future research should focus on improving the selectivity through effective strategies such as optimizing the structure and composition of the sensing materials, *e.g.*, surface functionalization and building MOS@MOFs structures. Moreover, researchers should focus on developing new design strategies to further optimize the application of metal oxides for gas sensing using novel 2D nanomaterials (e.g., MXene[148]), which sensing mechanisms have not been fully elucidated and still need to be further explored. In addition, most of the gas sensors reported in laboratories can detect ppm or sub-ppm level gases. But some applications, *e.g.*, respiratory diagnostics, industrial inspection, *etc.*, require higher sensitivity sensors that extend the detection limit to ppb or even ppq. Therefore, it is essential to seek effective ways to improve sensor sensitivity, *e.g.*, UV light irradiation.

(2) Despite advancements in sensor arrays with machine learning, the integration of sensors with diverse operating principles remains underexplored and overlooked. The

flexibility and performance of systems can be significantly enhanced by combining MOS sensors with different types of sensors, such as electrochemical sensors, photoionization detection sensors, catalytic sensors, and combustible sensors. Thus, the system can meet the requirements of diversified targets and realize high sensitivity and selective detection of multiple gases. In addition, the miniaturization of smart electronic nose systems still faces many challenges. Significant research efforts, including advancements in microelectromechanical systems technology, have been dedicated to miniaturizing gas sensors and enabling system integration. Advancements optimize sensor configurations, enhancing algorithm accuracy and reducing training costs, paving the way for portable, miniaturized electronic noses.

(3) Gas sensing performance improvement studies often focus narrowly on specific aspects, such as enhancing sensitivity or response speed. While these isolated approaches may achieve progress in laboratory settings, they struggle to address the complex and dynamic demands of real-world applications. The key to advancing sensor technology commercialization lies in establishing a comprehensive, high-quality platform that integrates chemical, mechanical, and biological sensing to deliver multidimensional information support. In this context, machine learning algorithms are expected to play a key role in the design of complex systems. And analyzing data, optimizing sensor array performance, and accelerating adoption across diverse applications. Beyond data processing in smart e-nose systems, machine learning can influence the design phase, including sensor configuration and material selection. By leveraging reverse design, machine learning can identify ideal materials with desired functionalities and optimize sensing configurations, enabling compact, efficient implementations.

As sensing materials, sensors, microprocessor units, and computational technologies continue to improve, machine learning will assist MOS gas sensor arrays to show even greater benefits for commercialization, ranging from environmental monitoring, medical testing, food safety, and other related fields.

Data availability

No primary research results, software or code have been included and no new data were generated or analysed as part of this review.

Conflicts of interest

There are no conflicts to declare.

Acknowledgements

This work was supported by the National Key Research and Development Program of China (2022YFB3203500), the National Natural Science Foundation of China [Grant No. 62471460, 62431026, 62301544, 22125803].

Notes and references

1 M. Yan, J. Chen, B. Wang, B. Li, H. Liu, W. Xu, H. Cao, Y. Fu, Q. He and J. Cheng, *Sens. Actuators, B*, 2022, **358**, 131519.
2 O. Djedidi, M. A. Djeziri, N. Morati, J.-L. Seguin, M. Bendahan and T. Contaret, *Sens. Actuators, B*, 2021, **339**, 129817.
3 K. Li, L. Wang, J. Chen, M. Yan, Y. Fu, Q. He and J. Cheng, *Sens. Actuators, B*, 2021, **334**, 129629.
4 Z. Zhu, H. Liu, P. Ding, Y. Fu, H. Cao, W. Xu, Q. He and J. Cheng, *ACS Sens.*, 2023, **8**, 1318–1327.
5 J.-H. Zhao, W.-X. Xu, B. Li, W. Xu, W.-K. Zhang, M.-S. Yuan, H.-Z. Li, Q.-G. He, X. Ma, J.-G. Cheng and Y.-Y. Fu, *Chin. Chem. Lett.*, 2024, **35**, 108579.
6 C. Cai, J. Mo, Y. Lu, N. Zhang, Z. Wu, S. Wang and S. Nie, *Nano Energy*, 2021, **83**, 105833.
7 K.-R. Park, J. Kwon and H. Choi, *J. Mater. Chem. C*, 2024, **12**, 15895–15902.
8 A. T. Güntner, M. Righettoni and S. E. Pratsinis, *Sens. Actuators, B*, 2016, **223**, 266–273.
9 M. Aliramezani, A. Norouzi and C. R. Koch, *Sens. Actuators, B*, 2020, **321**, 128414.
10 J. Chen, M. Yan, Y. Tang, J. Yu, W. Xu, Y. Fu, H. Cao, Q. He and J. Cheng, *ACS Appl. Bio Mater.*, 2019, **2**, 3678–3685.
11 Z. Shen, W. Huang, L. Li, H. Li, J. Huang, J. Cheng and Y. Fu, *Small*, 2023, **19**, 2302406.
12 M. Wu, S. Hou, X. Yu and J. Yu, *J. Mater. Chem. C*, 2020, **8**, 13482–13500.
13 Z. Shen, W. Li, W. Tang, X. Jiang, K. Qi, H. Liu, W. Xu, W. Xu, S. Zang, K. Zhen, H. Li, Q. He, M. Tu, J. Cheng, Z. Fan and Y. Fu, *Adv. Funct. Mater.*, 2024, **34**, 2401631.
14 W. Lv, J. Yang, Q. Xu, J. A.-A. Mehrez, J. Shi, W. Quan, H. Luo, M. Zeng, N. Hu, T. Wang, H. Wei and Z. Yang, *Nat. Commun.*, 2024, **15**, 6936.
15 R. Dong, Z. Shen, H. Li, J. Cheng and Y. Fu, *J. Mater. Chem. C*, 2024, **12**, 12692–12707.
16 T. Fan, W. Xu, J. Yao, Z. Jiao, Y. Fu, D. Zhu, Q. He, H. Cao and J. Cheng, *ACS Sens.*, 2016, **1**, 312–317.
17 L. Chen, Y. Gao, Y. Fu, D. Zhu, Q. He, H. Cao and J. Cheng, *RSC Adv.*, 2015, **5**, 29624–29630.
18 J. Tang, J. Fang, Y. Liang, B. Zhang, Y. Luo, X. Liu, Z. Li, X. Cai, J. Xian, H. Lin, W. Zhu, H. Guan, H. Lu, J. Zhang, J. Yu and Z. Chen, *Sens. Actuators, B*, 2018, **273**, 1816–1826.
19 Z. Zhou, Y. Xu, C. Qiao, L. Liu and Y. Jia, *Sens. Actuators, B*, 2021, **332**, 129482.
20 S. Zeinali, S. Homayoonnia and G. Homayoonnia, *Sens. Actuators, B*, 2019, **278**, 153–164.
21 C. Wu, L. Han, J. Zhang, Y. Wang, R. Wang and L. Chen, *Adv. Mater. Technol.*, 2022, **7**, 2101247.
22 M. Xiao, S. Liang, J. Han, D. Zhong, J. Liu, Z. Zhang and L. Peng, *ACS Sens.*, 2018, **3**, 749–756.
23 S. Su and J. Hu, *ACS Sens.*, 2019, **4**, 2491–2496.
24 Z. Yuan, E. Han, F. Meng and K. Zuo, *IEEE Trans. Instrum. Meas.*, 2020, **69**, 4533–4544.
25 J. Wang, W. Gu, W. Qi, C. Li, D. Chen, G. Adedokun, L. Xu and F. Wu, *IEEE Sens. J.*, 2021, **21**, 6821–6829.

26 Z. Han, Y. Qi, Z. Yang, H. Han, Y. Jiang, W. Du, X. Zhang, J. Zhang, Z. Dai, L. Wu, C. Fletcher, Z. Wang, J. Liu, G. Lu and F. Wang, *J. Mater. Chem. C*, 2020, **8**, 13169–13188.
27 S. Uma and M. K. Shobana, *Sens. Actuators, A*, 2023, **349**, 114044.
28 Q. Zhou, S. Luo, W. Xue and N. Liao, *Chem. Eng. J.*, 2023, **475**, 146318.
29 J. Chu, Q. Wang, Y. Liu, J. Pan, H. Yuan, A. Yang, X. Wang and M. Rong, *IEEE Trans. Power Delivery*, 2023, **38**, 222–230.
30 L. Zhang and D. Zhang, *IEEE Trans. Syst. Man Cybern. Syst.*, 2018, **48**, 242–254.
31 T. Seesaard, N. Goel, M. Kumar and C. Wongchoosuk, *Comput. Electron. Agric.*, 2022, **193**, 106673.
32 N. D. Pinheiro, R. T. Freire, J. A. M. Conrado, A. D. Batista and J. F. Da Silveira Petruci, *Anal. Chim. Acta*, 2021, **1143**, 1–8.
33 H. Zhao, L. Liu, X. Lin, J. Dai, S. Liu, T. Fei and T. Zhang, *ACS Sens.*, 2020, **5**, 346–352.
34 A. Amini and M. Vafaei, *IEEE Sens. J.*, 2020, **20**, 13220–13228.
35 H. Tai, S. Wang, Z. Duan and Y. Jiang, *Sens. Actuators, B*, 2020, **318**, 128104.
36 C. C. Moor, J. C. Oppenheimer, G. Nakshbandi, J. G. J. V. Aerts, P. Brinkman, A.-H. Maitland-van Der Zee and M. S. Wijsenbeek, *Eur. Respir. J.*, 2021, **57**, 2002042.
37 A. I. F. Al Isyrofie, M. Kashif, A. K. Aji, N. Aidatuzzahro, A. Rahmatillah, Winarno, Y. Susilo, A. Syahrom and S. D. Astuti, *Sens. Bio-Sens. Res.*, 2022, **37**, 100508.
38 J. Han, M. Kang, J. Jeong, I. Cho, J. Yu, K. Yoon, I. Park and Y. Choi, *Adv. Sci.*, 2022, **9**, 2106017.
39 H. Wang, Z. Zhao, Z. Wang, G. Xu and L. Wang, *IEEE Trans. Ind. Inform.*, 2020, **16**, 2698–2706.
40 C. Wang, Z. Chen, C. L. J. Chan, Z. Wan, W. Ye, W. Tang, Z. Ma, B. Ren, D. Zhang, Z. Song, Y. Ding, Z. Long, S. Poddar, W. Zhang, Z. Wan, F. Xue, S. Ma, Q. Zhou, G. Lu, K. Liu and Z. Fan, *Nat. Electron.*, 2024, **7**, 157–167.
41 H. Mei, J. Peng, T. Wang, T. Zhou, H. Zhao, T. Zhang and Z. Yang, *Nano-Micro Lett.*, 2024, **16**, 269.
42 W. Ni, T. Wang, Y. Wu, X. Liu, Z. Li, R. Yang, K. Zhang, J. Yang, M. Zeng, N. Hu, B. Li and Z. Yang, *Sens. Actuators, B*, 2024, **417**, 136206.
43 R. Gao, S. Gao, P. Wang, Y. Xu, X. Zhang, X. Cheng, X. Zhou, Z. Major, H. Zhu and L. Huo, *Sens. Actuators, B*, 2020, **303**, 127085.
44 D. Zhang, Q. Mi, D. Wang and T. Li, *Sens. Actuators, B*, 2021, **339**, 129923.
45 R. Paul, B. Das and R. Ghosh, *J. Alloys Compd.*, 2023, **941**, 168943.
46 D. Wong, O. Abuzalat, S. Mostafa, S. S. Park and S. Kim, *J. Mater. Chem. C*, 2020, **8**, 7567–7574.
47 X. San, M. Li, D. Liu, G. Wang, Y. Shen, D. Meng and F. Meng, *J. Alloys Compd.*, 2018, **739**, 260–269.
48 X.-T. Yin, D. Dastan, F. Gity, J. Li, Z. Shi, N. D. Alharbi, Y. Liu, X.-M. Tan, X.-C. Gao, X.-G. Ma and L. Ansari, *Sens. Actuators, A*, 2023, **354**, 114273.
49 M. Guo, N. Luo, Y. Chen, Y. Fan, X. Wang and J. Xu, *J. Hazard. Mater.*, 2022, **429**, 127471.
50 T. Seiyama, A. Kato, K. Fujiishi and M. Nagatani, *Anal. Chem.*, 1962, **34**, 1502–1503.
51 M. Fois, T. Cox, N. Ratcliffe and B. De Lacy Costello, *Sens. Actuators, B*, 2021, **330**, 129264.
52 A. Bora, J. George, Y. Sivalingam, V. J. Surya, G. Magna, S. R. N. K. Mangalampalli, R. Paolesse and C. Di Natale, *J. Mater. Chem. C*, 2024, **12**, 9968–9977.
53 K. G. Krishna, G. Umadevi, S. Parne and N. Pothukanuri, *J. Mater. Chem. C*, 2023, **11**, 3906–3925.
54 W. Wei, J. Zhao, S. Shi, H. Lin, Z. Mao, F. Zhang and F. Qu, *J. Mater. Chem. C*, 2020, **8**, 6734–6742.
55 M. Sik Choi, M. Young Kim, A. Mirzaei, H.-S. Kim, S. Kim, S.-H. Baek, D. Won Chun, C. Jin and K. Hyoung Lee, *Appl. Surf. Sci.*, 2021, **568**, 150910.
56 P. Cao, Y. Cai, D. Pawar, S. Han, W. Xu, M. Fang, X. Liu, Y. Zeng, W. Liu, Y. Lu and D. Zhu, *J. Mater. Chem. C*, 2022, **10**, 4295–4305.
57 X. Liu, M. Zhou, S. Zhang, S. Cao, G. Lei, C. Lou and J. Zhang, *J. Hazard. Mater.*, 2021, **415**, 125757.
58 J. Wang, S. Fan, Y. Xia, C. Yang and S. Komarneni, *J. Hazard. Mater.*, 2020, **381**, 120919.
59 J. Liu, L. Zhang, J. Fan, B. Zhu and J. Yu, *Sens. Actuators, B*, 2021, **331**, 129425.
60 N. T. Riek, S. So, M. Akcakaya and M. Yun, *IEEE Sens. J.*, 2022, **22**, 19136–19143.
61 S. Kim, G. Singh, M. Oh and K. Lee, *ACS Sens.*, 2021, **6**, 4145–4155.
62 V. V. Krivetskiy, M. D. Andreev, A. O. Efitorov and A. M. Gaskov, *Sens. Actuators, B*, 2021, **329**, 129187.
63 W. Tang, Z. Chen, Z. Song, C. Wang, Z. Wan, C. L. J. Chan, Z. Chen, W. Ye and Z. Fan, *ACS Nano*, 2022, **16**, 10968–10978.
64 M. Zhan, C. Ge, S. Hussain, A. S. Alkorbi, R. Alsaiari, N. A. Alhemiary, G. Qiao and G. Liu, *Chemosphere*, 2022, **291**, 132842.
65 Y. Masuda, *Sens. Actuators, B*, 2022, **364**, 131876.
66 N. Wang, Z. Liu, Y. Zhou, L. Zhao, X. Kou, T. Wang, Y. Wang, P. Sun and G. Lu, *Small*, 2024, **20**, 2310465.
67 W. Pi, X. Chen, Q. Fu, Z. Lu, H. Li, Z. Tang and W. Luo, *J. Mater. Chem. C*, 2023, **11**, 12517–12524.
68 Y. Li, N. Luo, W. Zhang, Q. Hu, X. Wang, Y. Chen, Z. Cheng and J. Xu, *J. Mater. Chem. C*, 2020, **8**, 12418–12426.
69 Z. Zhang, L. Luo, Y. Zhang, G. Lv, Y. Luo and G. Duan, *Adv. Sci.*, 2023, **10**, 2302614.
70 B. Feng, Y. Feng, Y. Li, Y. Su, Y. Deng and J. Wei, *ACS Sens.*, 2022, **7**, 3963–3972.
71 J. Li, M. Yang, X. Cheng, X. Zhang, C. Guo, Y. Xu, S. Gao, Z. Major, H. Zhao and L. Huo, *J. Hazard. Mater.*, 2021, **419**, 126414.
72 A. Liu, S. Lv, L. Jiang, F. Liu, L. Zhao, J. Wang, X. Hu, Z. Yang, J. He, C. Wang, X. Yan, P. Sun, K. Shimanoe and G. Lu, *Sens. Actuators, B*, 2021, **332**, 129444.
73 L. Song, L. Yang, Z. Wang, D. Liu, L. Luo, X. Zhu, Y. Xi, Z. Yang, N. Han, F. Wang and Y. Chen, *Sens. Actuators, B*, 2019, **283**, 793–801.

74 J. Lee, Y. Jung, S.-H. Sung, G. Lee, J. Kim, J. Seong, Y.-S. Shim, S. C. Jun and S. Jeon, *J. Mater. Chem. A*, 2021, **9**, 1159–1167.
75 H. Bi, Y. Shen, S. Zhao, P. Zhou, S. Gao, B. Cui, D. Wei, Y. Zhang and K. Wei, *Vacuum*, 2020, **172**, 109086.
76 W. Du, W. Si, F. Wang, L. Lv, L. Wu, Z. Wang, J. Liu and W. Liu, *Sens. Actuators, B*, 2020, **303**, 127221.
77 L. Gao, Z. Cheng, Q. Xiang, Y. Zhang and J. Xu, *Sens. Actuators, B*, 2015, **208**, 436–443.
78 Y. Liu, X. Liu, Y. Wang, R. Wang and T. Zhang, *Ceram. Int.*, 2019, **45**, 9820–9828.
79 Q. Ma, S. Chu, H. Li, J. Guo, Q. Zhang and Z. Lin, *Appl. Surf. Sci.*, 2021, **569**, 151074.
80 Y. Zhao, S. Wang, W. Yuan, S. Fan, Z. Hua, Y. Wu and X. Tian, *Sens. Actuators, B*, 2021, **328**, 129030.
81 W. Bu, N. Liu, Y. Zhang, W. Han, X. Chuai, Z. Zhou, C. Hu and G. Lu, *Sens. Actuators, B*, 2024, **404**, 135260.
82 B. Liu, L. Zhang, Y. Luo, L. Gao and G. Duan, *Small*, 2021, **17**, 2105643.
83 J. Oh, S. H. Kim, M.-J. Lee, H. Hwang, W. Ku, J. Lim, I.-S. Hwang, J.-H. Lee and J.-H. Hwang, *Sens. Actuators, B*, 2022, **364**, 131894.
84 D. Kwon, G. Jung, W. Shin, Y. Jeong, S. Hong, S. Oh, J.-H. Bae, B.-G. Park and J.-H. Lee, *Sens. Actuators, B*, 2021, **340**, 129258.
85 Z. Otgonbayar, Y. J. Joo, K. Y. Cho, S. Y. Park, K. Y. Park and W.-C. Oh, *J. Mater. Chem. C*, 2022, **10**, 12106–12124.
86 X. Zhang, D. Song, Q. Liu, R. Chen, J. Hou, J. Liu, H. Zhang, J. Yu, P. Liu and J. Wang, *J. Mater. Chem. C*, 2019, **7**, 7219–7229.
87 S. Li, L. Xie, M. He, X. Hu, G. Luo, C. Chen and Z. Zhu, *Sens. Actuators, B*, 2020, **310**, 127828.
88 K. Zhang, S. Qin, P. Tang, Y. Feng and D. Li, *J. Hazard. Mater.*, 2020, **391**, 122191.
89 C. Dong, R. Zhao, L. Yao, Y. Ran, X. Zhang and Y. Wang, *J. Alloys Compd.*, 2020, **820**, 153194.
90 S. Acharyya, S. Nag and P. K. Guha, *IEEE Sens. J.*, 2021, **21**, 5771–5778.
91 Y. Fan, K. Li, X. Ren, W. Yan, C. Zhu, Y. Zhao, W. Zeng, Z. Chen and S. Wang, *J. Mater. Chem. C*, 2021, **9**, 17496–17503.
92 J. Park and H. Tabata, *ACS Omega*, 2021, **6**, 21284–21293.
93 H. Bai, H. Guo, C. Feng, J. Wang, B. Liu, Z. Xie, F. Guo, D. Chen, R. Zhang and Y. Zheng, *J. Mater. Chem. C*, 2022, **10**, 3756–3769.
94 L. Yin, G. Qu, P. Guo, R. Zhang, J. Sun and D. Chen, *J. Alloys Compd.*, 2019, **785**, 367–373.
95 N. Wang, W. Tao, X. Gong, L. Zhao, T. Wang, L. Zhao, F. Liu, X. Liu, P. Sun and G. Lu, *Sens. Actuators, B*, 2022, **362**, 131803.
96 L. Sui, T. Yu, D. Zhao, X. Cheng, X. Zhang, P. Wang, Y. Xu, S. Gao, H. Zhao, Y. Gao and L. Huo, *J. Hazard. Mater.*, 2020, **385**, 121570.
97 F. Abegaz, K. Chaichoompu, E. Génin, D. W. Fardo, I. R. König, J. M. Mahachie John and K. Van Steen, *Brief. Bioinform.*, 2019, **20**, 2200–2216.
98 M. Shooshtari and A. Salehi, *Sens. Actuators, B*, 2022, **357**, 131418.
99 A. Filianoti, M. Costantini, A. M. Bove, U. Anceschi, A. Brassetti, M. Ferriero, R. Mastroianni, L. Misuraca, G. Tuderti, G. Ciliberto and G. Simone, *Cancers*, 2022, **14**, 2927.
100 E. Núñez-Carmona, M. Abbatangelo, I. Zottele, P. Piccoli, A. Tamanini, E. Comini, G. Sberveglieri and V. Sberveglieri, *Foods*, 2019, **8**, 632.
101 T. Itoh, Y. Koyama, Y. Sakumura, T. Akamatsu, A. Tsuruta, Y. Masuda and W. Shin, *Sens. Actuators, B*, 2023, **387**, 133803.
102 Z. Cao, Y. Ge, W. Wang, J. Sheng, Z. Zhang, J. Li, Y. Sun and F. Dong, *ACS Sens.*, 2022, **7**, 1757–1765.
103 F. Meng, H. Ji, Z. Yuan, Y. Chen, H. Zhang, W. Qin and H. Gao, *IEEE Sens. J.*, 2021, **21**, 10915–10922.
104 N. Gerhardt, S. Schwolow, S. Rohn, P. R. Pérez-Cacho, H. Galán-Soldevilla, L. Arce and P. Weller, *Food Chem.*, 2019, **278**, 720–728.
105 Z. Wu, H. Zhang, H. Ji, Z. Yuan and F. Meng, *J. Alloys Compd.*, 2022, **918**, 165510.
106 B. Wang, L. Huang, J. Zhang, Q. Lu, S. Zhang, W. Li, T. Wang, H. Sun, X. Liang, F. Liu, P. Sun and G. Lu, *IEEE Electron Device Lett.*, 2022, **43**, 1736–1739.
107 J. Yun, C. Cui, S. Zhang, J. Zhu, C. Peng, H. Cai, X. Yang and R. Hou, *Food Chem.*, 2021, **360**, 130033.
108 S. Kanaparthi and S. G. Singh, *Sens. Actuators, B*, 2021, **348**, 130725.
109 B. Wang, J. Zhang, T. Wang, W. Li, Q. Lu, H. Sun, L. Huang, X. Liang, F. Liu, F. Liu, P. Sun and G. Lu, *ACS Appl. Mater. Interfaces*, 2023, **15**, 6047–6057.
110 S.-H. Wang, T.-I. Chou, S.-W. Chiu and K.-T. Tang, *IEEE Sens. J.*, 2021, **21**, 6401–6407.
111 K. Geng, J. M. Ata, J. Chen, J. Hu and H. Zhang, in *Proceedings of the 2023 2nd Asia Conference on Algorithms, Computing and Machine Learning*, ACM, Shanghai China, 2023, pp. 247–252.
112 X. Zhai, A. A. S. Ali, A. Amira and F. Bensaali, *IEEE Access*, 2016, **4**, 8138–8146.
113 H. Song, L. Ma, S. Pei, C. Dong, E. Zhu and B. Zhang, *Sens. Actuators, A*, 2021, **331**, 112940.
114 Z. Wang, C. Xie, B. Liu, Y. Jiang, Z. Li, H. Tai and X. Li, *Sens. Actuators, B*, 2022, **362**, 131812.
115 S. Lin, Y. Zhou, J. Hu, Z. Sun, T. Zhang and M. Wang, *Sens. Actuators, B*, 2022, **362**, 131733.
116 Z. Li, J. Yu, D. Dong, G. Yao, G. Wei, A. He, H. Wu, H. Zhu, Z. Huang and Z. Tang, *Sens. Actuators, B*, 2023, **380**, 133289.
117 V. Pareek, S. Chaudhury and S. Singh, *IEEE Sens. J.*, 2021, **21**, 24263–24273.
118 J. Pan, A. Yang, D. Wang, J. Chu, F. Lei, X. Wang and M. Rong, *IEEE Trans. Instrum. Meas.*, 2022, **71**, 1–8.
119 W. Zhang, L. Wang, J. Chen, X. Bi, C. Chen, J. Zhang and V. Hans, *IEEE Sens. J.*, 2021, **21**, 18459–18468.
120 M. Kang, I. Cho, J. Park, J. Jeong, K. Lee, B. Lee, D. Del Orbe Henriquez, K. Yoon and I. Park, *ACS Sens.*, 2022, **7**, 430–440.

121 C. Zhan, J. He, M. Pan and D. Luo, *Sensors*, 2021, **21**, 347.
122 Y. Song, J. Zhao, X. Zhang, M. Yang, B. Yu, Y. Ma, S. Zhou and J. Li, *Sens. Actuators, B*, 2024, **401**, 135071.
123 L. Han, C. Yu, K. Xiao and X. Zhao, *Sensors*, 2019, **19**, 1960.
124 G. Wei, G. Li, J. Zhao and A. He, *Sensors*, 2019, **19**, 217.
125 Y. Yang, S. Lin and J. Hu, *Sens. Actuators, B*, 2023, **385**, 133721.
126 Y. Guo, M. Yang, G. Huang and Y. Zheng, *Chem. Eng. J.*, 2024, **492**, 152280.
127 W. Ren, C. Zhao, G. Niu, Y. Zhuang and F. Wang, *Adv. Intell. Syst.*, 2022, **4**, 2200169.
128 J. Chu, W. Li, X. Yang, Y. Wu, D. Wang, A. Yang, H. Yuan, X. Wang, Y. Li and M. Rong, *Sens. Actuators, B*, 2021, **329**, 129090.
129 O. Attallah and I. Morsi, *Measurement*, 2022, **199**, 111458.
130 L. Mahmood, Z. Bahroun, M. Ghommem and H. Alshraideh, *Facta Univ. Ser. Mech. Eng.*, 2022, **20**, 479.
131 U. Javed, K. P. Ramaiyan, C. R. Kreller, E. L. Brosha, R. Mukundan, A. M. Sengupta and A. V. Morozov, *Sens. Actuators, B*, 2022, **359**, 131589.
132 Z. Wang, W. Chen, S. Gu, J. Wang and Y. Wang, *Sens. Actuators, B*, 2020, **309**, 127767.
133 T. Zhang, R. Tan, W. Shen, D. Lv, J. Yin, W. Chen, H. Fu and W. Song, *Sens. Actuators, B*, 2023, **382**, 133555.
134 H. Zhu, C. Liu, Y. Zheng, J. Zhao and L. Li, *IEEE Sens. J.*, 2023, **23**, 2940–2947.
135 S. Dragonieri, M. D. Marco, M. Ahroud, V. N. Quaranta, A. Portacci, I. Iorillo, F. Montagnolo and G. E. Carpagnano, *J. Breath Res.*, 2024, **18**, 036006.
136 T. Saidi, M. Moufid, K. De Jesus Beleño-Saenz, T. G. Welearegay, N. El Bari, A. Lisset Jaimes-Mogollon, R. Ionescu, J. E. Bourkadi, J. Benamor, M. El Ftouh and B. Bouchikhi, *Sens. Actuators, B*, 2020, **311**, 127932.
137 B. Liu, H. Yu, X. Zeng, D. Zhang, J. Gong, L. Tian, J. Qian, L. Zhao, S. Zhang and R. Liu, *Sens. Actuators, B*, 2021, **339**, 129896.
138 J. Chen, L. Wang and S. Duan, *Neurocomputing*, 2021, **461**, 129–136.
139 B. V. Abraham, M. Subramoniam and L. Mathew, *Expert Rev. Mol. Diagn.*, 2021, **21**, 1223–1233.
140 J. C. Rodriguez Gamboa, E. S. Albarracin E, A. J. Da Silva, L. L. De Andrade Lima and T. A. E. Ferreira, *LWT*, 2019, **108**, 377–384.
141 C. Gonzalez Viejo, S. Fuentes, A. Godbole, B. Widdicombe and R. R. Unnithan, *Sens. Actuators, B*, 2020, **308**, 127688.
142 M. Zhou, R. Khir, Z. Pan, J. F. Campbell, R. Mutters and Z. Hu, *J. Stored Prod. Res.*, 2021, **92**, 101805.
143 M. Rasekh, H. Karami, A. D. Wilson and M. Gancarz, *Chemosensors*, 2021, **9**, 142.
144 W. Jia, G. Liang, H. Tian, J. Sun and C. Wan, *Sensors*, 2019, **19**, 1526.
145 S. D. Astuti, M. H. Tamimi, A. A. S. Pradhana, K. A. Alamsyah, H. Purnobasuki, M. Khasanah, Y. Susilo, K. Triyana, M. Kashif and A. Syahrom, *Biosens. Bioelectron. X*, 2021, **9**, 100083.
146 Y. Zhuang, D. Yin, L. Wu, G. Niu and F. Wang, *APL Mach. Learn.*, 2024, **2**, 016104.
147 S. Liu, X. Chen, X. Xia, Y. Jin, G. Wang, H. Jia and D. Huang, *Comput. Electron. Agric.*, 2024, **221**, 108947.
148 W. Quan, J. Shi, M. Zeng, W. Lv, X. Chen, C. Fan, Y. Zhang, Z. Liu, X. Huang, J. Yang, N. Hu, T. Wang and Z. Yang, *Nano-Micro Lett.*, 2024, **16**, 277.